Surface Jumping: $S_2 \rightarrow S_0$ Internal Conversion in Benzene

S. Kallush[1] B. Segev[1] A. Sergeev[1]and E.J. Heller[2]
1 *Department of Chemistry, Ben-Gurion University of the Negev, POB 653, Beer-Sheva 84105, ISRAEL*
2 *Departments of Chemistry and Physics, Harvard University, Cambridge, MA 02138 USA*

We generalize the concept of Tully-Preston surface hopping to include larger *jumps* in the case that the surfaces do not cross. Instead of identifying a complex hopping point, we specify a jump between two locales in phase space. This concept is used here to find propensity rules for the accepting vibrational mode(s) in a radiationless vibronic relaxation transition. As an application, we consider the classic problem of $S_2 \rightarrow S_0$ vibronic relaxation transition of the benzene molecule where 30 modes of vibration compete for the electronic energy. Given the energy gap, reasonable displacements and recently calculated force fields we show that the surface jumping involves the jump in coordinate space of a single $C-H$ local stretching mode of the hydrogen atom toward the ring.

I. INTRODUCTION

Molecular electronic transitions may be radiative or non-radiative. In either case, the process may be Franck-Condon allowed or supressed. The allowed processes correspond to a crossing of Born-Oppenheimer potential energy surfaces in the classically accesible region, whereas Franck-Condon supressed events have no such crossing. Examples include radiative processes in the wings of absorption or emission band envelopes, and radiationless events for nested potential energy surfaces.

We focus here on intuition and procedures for realistic polyatomic processes. For the case of surface crossing, the Tully-Preston surface hopping [1] picture has been of considerable value, permitting both intuition and simple procedures for calculating rates of electronic conversion. When the surfaces cross, trajectories can hop smoothly with little or no change in position or momentum at the time of the hop. But often surfaces do not cross. What then? Of course, the rate for such cases is generally lower because of the implied supression of Franck-Condon factors. However, these supressed events may be "the only game in town" or may be significant channels competing with others. Analytical continuation is sometimes used in these cases to recognize a complex jumping point in coordinate space [2–4], but we want a more direct procedure which is applicable to many degrees of freedom. The aproach we use is surface jumping [5].

Our paradigm in this paper is a radiationless transition between nested surface potentials as shown in figure 1(b). This situation can also arise radiatively, if we consider say the upper surface to be raised past the absorption maximum by the photon energy $h\nu$ as in figure 1(d). We have in mind a many coordinate example.

Perhaps it is not obvious that any useful classical picture can emerge for this noncrossing situation, since the situation we describe is classically forbidden. However, other classically forbidden processes have very useful classical descriptions, such as barrier tunneling, which involves trajectories in imaginary time or on the inverted potential energy surface. Recently, some of us have outlined a procedure to recognize the jumping points in phase space in the noncrossing regime [5,6]. We have shown, and demonstrated for a harmonic model, that identification of the jumping points enables easy derivation of propensity rules for the distribution of the electronic energy between competing vibrational modes [5]. Here we present the first application of this phase-space method to a realistic complex physical system, the 30 modes problem of the $S_2 \rightarrow S_0$ transition of the benzene molecule [7–11]. The transition takes place through non-radiative internal conversion and a large energy of 0.228 eV is released to the vibrational degrees of freedom of the ground S_0 state. The two surfaces do not cross in a classically allowed region and a quantum jump must take place. For the example of the $S_2 \rightarrow S_0$ transition in the benzene molecule it is certainly not trivial to determine which modes or combination of the 30 vibrational modes would be first excited during the quantum jump.

Questions that we address in this paper are:

- Where will the jump between the two surfaces take place?
- What is the best system of coordinates to describe the process?
- What is the sensitivity of these predictions to the value of various parameters?

The outline of the paper is as follows: Surface jumping is defined and analyzed in section II. In section III we review the known and unknown

experimental and theoretical data regarding the $S_2 \rightarrow S_0$ transition of the benzene molecule. In section IV we apply the method of section II to the process described in section III using only known parameters and making the simplest conjectures for the unknown parameters. Section V discusses the sensitivity of the results to the unknown data regarding the S_2 surface potential. Section VI concludes and summarizes.

II. THE PHASE SPACE APPROACH FOR ANALYZING FRANK-CONDON FACTORS

A. Quantum-mechanical treatment in coordinate space

The probability for an allowed transition from the vibronic state i to a vibronic manifold j, where i, j refer to electronic states is given by:

$$P^{i\rightarrow j} = |\mu_{elec}|^2 \sum_{\left\{n'_k\right\}} \prod_k \left| \left\langle \chi^j_{n'_k} | \chi^i_{n_k} \right\rangle \right|^2 , \quad (1)$$

Here $\mu_{elec} = \int \psi^*_j \hat{\mu}_{elec} \psi_i d\,\vec{r}$, is the dipole transition moment between the electronic states ψ_i and ψ_j and $\hat{\mu}_{elec}$ is the dipole moment operator. The integration $d\vec{r}$ is over all the electronic coordinates $\vec{r}$. The nuclear wave function for the mode q_k in the electronic state i for vibrationally excited state n_k is $\chi^i_{n_k}$, and separability is assumed. Separability is not necessary for our approach, and we do not use it below for the final state, but here we use it for simplicity. The term $\prod_k \left| \left\langle \chi^j_{n'_k} | \chi^i_{n_k} \right\rangle \right|^2$ in this expression is the FC factor squared between two vibronic states. The summation, $\sum_{\left\{n'_k\right\}}$, is over a manifold of vibronic states, whose energy is equal to the energy of the initial state i. Note that an excited initial state, as considered here, has a finite energy width allowing for many final states with slightly different energies. For electronically forbidden transition $\mu_{elec} = 0$ at the equilibrium position. Nevertheless, the transition can occur by nonadiabatic coupling via the kinetic energy operator. The probability for an electronically forbidden transition from the vibronic state i to another vibronic manifold j is:

$$P^{i\rightarrow j} = \sum_{\mathsf{p}} |M^{\mathsf{p}}_{elec}|^2 \sum_{n'_{\mathsf{p}}} \left| \left\langle \chi^j_{n'_{\mathsf{p}}} | \frac{\partial}{\partial q_{\mathsf{p}}} | \chi^i_{n_{\mathsf{p}}} \right\rangle \right|^2 \sum_{\left\{n'_k \neq n'_{\mathsf{p}}\right\}} \prod_{k\neq \mathsf{p}} \left| \left\langle \chi^j_{n'_k} | \chi^i_{n_k} \right\rangle \right|^2 \quad (2)$$

Here, $M_{elec} = \left\langle \psi^j | \frac{\partial}{\partial q_{\mathsf{p}}} | \psi^i \right\rangle$ is the non-adiabatic interaction matrix element while p serves as the promoting vibration of the normal mode q_{p}. The promoting mode is the mode which couples between the electronic surfaces via its kinetic energy operator and therefore should have the correct symmetry to prevent the electronic matrix element M_e from vanishing. The sum over p takes into account all possible promoting modes. The last term in Eq. (2) is the FC factor squared for the nuclei subspace which includes all the nuclei coordinates except for the one which serves as the promoting mode with a summation over all the possible divisions of the vibrational energy between the modes. In both these cases, the FC factors strongly influence the transition probability and practically control the distribution of the electronic energy that is released in the relaxation process between the competing vibrational modes. It is useful to define the total FC factor squared as:

$$\Sigma_{I\rightarrow F} = \sum_{\left\{n'_k\right\}} \prod_k \left| \left\langle \chi^j_{n'_k} | \chi^i_{n_k} \right\rangle \right|^2 \quad (3)$$

for allowed transitions and:

$$\Sigma_{I\rightarrow F} = \sum_{n'_{\mathsf{p}}} \left| \left\langle \chi^j_{n'_{\mathsf{p}}} | \frac{\partial}{\partial q_{\mathsf{p}}} | \chi^i_{n_{\mathsf{p}}} \right\rangle \right|^2 \sum_{\left\{n'_k \neq n'_{\mathsf{p}}\right\}} \prod_{k\neq \mathsf{p}} \left| \left\langle \chi^j_{n'_k} | \chi^i_{n_k} \right\rangle \right|^2 \quad (4)$$

for forbidden transitions. Eqs. (3) and (4) were explicitly written for separable states. Generalization to non-separable states is straightforward as applied below.

The rate of the transition is given by Fermi golden rule:

$$\Gamma = \frac{2\pi\lambda^2}{\hbar} \rho_{final} \Sigma_{I\rightarrow F} \quad (5)$$

where ρ_{final} is the density of states on the ground electronic state (accepting surface) and λ^2 is the electronic part of either Eq. (1) or (2) for allowed or forbidden transitions, respectively. This rate can be written as the trace over two density matrixes: $\Gamma = \mathrm{Tr}\left[\hat{\rho}_f \hat{\rho}_i\right]\ 2\pi\lambda^2/\hbar$ for allowed transitions and $\Gamma = \mathrm{Tr}\left[\hat{\rho}_f \hat{\rho}'_i\right]\ 2\pi\lambda^2/\hbar$ for forbidden transitions, where

$$\hat{\rho}_{i\cdot} = \prod_k |\chi^i_{n_k}\rangle\langle\chi^i_{n_k}|, \quad (6)$$

ρ'_i is defined below, and

$$\hat{\rho}_F = \sum_{\{n'_k\}} \prod_k |\chi^j_{n'_k}\rangle\langle\chi^j_{n'_k}| \; \rho_{final} = \delta\left(\hat{H}_F - E\right), \tag{7}$$

where $\hat{H}_F$ is the Hamiltonian operator of the final electronic surface.

One way to determine which are the vibrations that are most likely to be excited is to calculate the different FC factors for all possible combinations of different divisions of the energy quanta between the modes. This, however, would demand an enormous computational effort and can be regarded as impossible for large molecules especially when the energy that is transferred between the degrees of freedom is large. Moreover, when the potential energy surface cannot be treated as separable, the eigenstates themselves are of mixed character and many will share roughly the same FC intensity, without revealing the mechanism or geometry of the jump between surfaces. Indeed, this can happen even for separable surfaces, in that many different final state FC factors could be comparable in size, reflecting the fact that the "jump" was not along any one of the separable coordinates.

B. Quantum-mechanical treatment in phase space

In the Wigner representation the total FC factors squared, multiplied by the final density of states, are expressed as an overlap *integral* in phase space. Our method for the derivation of propensity rules is based on recognizing the points in phase-space in which the FC *integrand* peaks. For convenience, we use an abridged form (q,p) for the nuclear positions and momenta for the set of normal modes $(\{q_k\},\{p_k\})$. In the Wigner phase space representation Γ takes the form:

$$\Gamma = \frac{2\pi\lambda^2}{\hbar}\int_{-\infty}^{\infty} dq \int_{-\infty}^{\infty} dp \; \rho_F(q,p) \; \rho_I(q,p), \tag{8}$$

for allowed transition. Here $\rho_I(q,p)$ and $\rho_F(q,p)$ are the Wigner functions of the initial and final states density matrices $\hat{\rho}_I$ and $\hat{\rho}_F$, respectively, defined in the usual way:

$$\rho(q,p) \equiv \frac{1}{2\pi\hbar}\int_{-\infty}^{\infty} d\eta \left\langle q + \frac{\eta}{2}|\hat{\rho}|q - \frac{\eta}{2}\right\rangle e^{-ip\eta/\hbar}. \tag{9}$$

Practically, we start with the description where each of the *initial* vibrational wave functions for each of the vibrational modes is characterizes by its quasi-distribution, i.e. we assume a separable system, for the excited electronic state. Consequently, the Wigner function $\rho_I(q,p)$ is a simple product of these well defined one dimensional quasi-distributions:

$$\rho_I(q,p) = \prod_k \rho^k_I(q_k,p_k)\,. \tag{10}$$

For a forbidden transition:

$$\Gamma = \sum_{\mathsf{p}} \Gamma_{\mathsf{p}}\,, \tag{11}$$

$$\Gamma_{\mathsf{p}} = \frac{2\pi\lambda^2}{\hbar}\int_{\infty}^{\infty} dq \int_{\infty}^{\infty} dp \; \rho_F(q,p) \; \rho_I^{(\mathsf{p})\prime}(q,p), \tag{12}$$

where the sum is over the promoting modes,

$$\rho_I^{(\mathsf{p})\prime}(q,p) \equiv \rho_I'^{\mathsf{p}}(q_{\mathsf{p}},p_{\mathsf{p}}) \prod_{k\neq\mathsf{p}} \rho^k_I(q_k,p_k)\,, \tag{13}$$

$$\rho_I'^{\mathsf{p}}(q_{\mathsf{p}},p_{\mathsf{p}}) \equiv \left[\hat{\rho}_I'^{\mathsf{p}}\right]_W = \left[\left|\frac{\partial\chi^i_{n_{\mathsf{p}}}}{\partial q_{\mathsf{p}}}\right\rangle\left\langle\frac{\partial\chi^i_{n_{\mathsf{p}}}}{\partial q_{\mathsf{p}}}\right|\right]_W, \tag{14}$$

and $[A]_W$ stands for the Wigner transform of A.

For the *final* state Wigner function, $\rho_F(q,p)$, a formal expression is obtained which substantially simplifies the calculation. For relaxation processes the final state (usually a quasi-continuum manifold of states) is defined by energy conservation to be given by the density matrix $\delta\left(\hat{H}_F - E\right)$. We define $\Delta(q,p)$ to be the Wigner transform of this Delta-function density and get

$$\Gamma = \frac{2\pi\lambda^2}{\hbar}\int dq \; dp \; \Delta(q,p)\rho_I(q,p), \tag{15}$$

for an allowed transition and

$$\Gamma_{\mathsf{p}} = \frac{2\pi\lambda^2}{\hbar}\sum_p \int dq \; dp \; \Delta(q,p)\rho_I^{(p)\prime}(q,p), \tag{16}$$

for a forbidden transition.

In our search for the direction of the surface jump we look for the point(s) or region(s) in phase-space (q^*,p^*) where the integrand, $\Delta(q,p)\rho_I(q,p)$, or $\Delta(q,p)\rho_I^{(\mathsf{p})'}(q,p)$, peaks.

C. Surface jumping

The Wigner function of the quasi-continuum final state $\Delta(q,p)$ can be expanded as an asymptotic power series in $\hbar$ [12–15]. A criterion for the validity of the asymptotic series expansion is given by:

$$\left(\frac{\hbar^2}{2m\left|\nabla V\right|}\right)^{1/3} < \sigma \tag{17}$$

where σ is the width of the initial wave function on the excited electronic surface, m is the reduced mass of the oscillator and $|\nabla V|$ is the magnitude of the gradient of the surface potential at the point of the transition. The zero order of this expansion which is in some sense a semiclassical approximation gives:

$$\Delta(q,p) \to \delta[E - H_F(q,p)] \tag{18}$$

where H_F is the classical Hamiltonian for the final (accepting) electronic state. Expansion to order $\hbar^2$ gives an Airy function instead of the delta function. An *exact* calculation of transition probabilities and rates may require more care, but the relative order of magnitudes of competing transitions as well as the partition of energy between competing accepting modes can be determined already at this semiclassical approximation level [16].

We are looking for the phase-space point(s) (q^*, p^*) where the integrand:

$$\delta[E - H_F(q,p)]\rho_I(q,p) \tag{19}$$

is maximal i.e. we maximize the initial Wigner function $\rho_I(q,p)$ under the constraint $E = H_F(q,p)$. (For forbidden transition $\rho_I(q,p)$ is replaced by $\rho_I^{(p)\prime}(q,p)$ throughout this analysis). The location of these points in phase-space gives us the phase-space jumping point(s) and from it we deduce an estimation for the energy distribution between competing modes. The value of $\rho_I(q,p)$ at these points indicates to the expected strength of the transition, although we emphasize again that predictions for absolute transition rates must be based on calculation of the *integral* and the electronic prefactors; here, we are finding the dominant pathway for radiationless transition.

The geometric interpretation of the problem is demonstrated in figure 2. The solid inner ellipses represent the contours of the Wigner function, here a gaussian, in some two dimensional space. The outer dashed curve is the energy surface constraint $H_F = E$. The geometric assignment is to find the points where the highest contour of the surface $\rho_I(q,p)$ meets the constraint hypersurface $E = H_F(q,p)$. As demonstrated in figure 2 the strength of the extremal points can vary. Panel (a) shows the case where the point of maximum of the Wigner function under the energy constraint is a *strong maximum*. In this case, there is a very rapid decrease of the Wigner function as one moves away from the extremum point on the energy constraint hypersurface. We can refer to the point as a *true* jumping point and use it to calculate expectation values like the relative amount of energy that goes into each of the modes [17]. Panel (b) stands as an example for a *weak* extremum. In this diagram the Wigner function contour and the energy constraint hypersurface have a very similar curvature. A decisive jumping point is not well defined.

D. Numerical considerations

The identification of the jumping point reduces in this formalism to the mathematical problem of finding the maximum of a multidimensional nonlinear objective function under a nonlinear constraint. Simple geometric considerations show that at all the extremum points:

$$\nabla H_F = \lambda \nabla \rho_I \ . \tag{20}$$

This condition gives a simple set of coupled algebraic equations whose roots define the local extrema. Note that direct multidimensional local minimum finding can be converted by various computational methods (like steepest decent) to a one-dimensional search. It is considered therefore to be a much easier computational problem than a multidimensional root search of a system of nonlinear equations [18]. However, numerical methods for local minima finding under a constraint appear to have difficulties in distinguishing between local minima, maxima, and saddle points. We therefore analyze the transition in two steps. We first use a code that takes the Wigner function and the ground electronic surface potential and uses a standard routine to find extremum points (q^*, p^*) of the Wigner function under the energy constraint, and the value of the Wigner function, $\rho_I\left(q^*, p^*\right)$, at these points. We then study the Wigner function on the constrained hypersurface at the vicinity of these points using algebraic considerations. The eigenvalues of a tensor of second derivatives in the subspace of the constrained phase space are calculated and the nature of each extremal point, be it a minimum, maximum, or saddle point is determined (see [17] for more details). For some cases, especially in the harmonic approximation, the problem is also solvable analytically. A detailed analytic analysis of the problem can be found in [5,17].

III. THE $S_2 \to S_0$ TRANSITION IN THE BENZENE MOLECULE

Transitions in the benzene molecule are one of the most investigated examples in molecular spectroscopy [7]. The transition from the ground state to the first two electronic states B_{2u} and B_{1u} is forbidden by symmetry. The vertical energy gap between the S_0 and S_2 state is 0.228 e.V. [7]. The $S_0 \to S_2$ absorption spectrum is very diffuse due to the non-adiabatic interactions and the quantum yield for the radiative transition is less then 1% in both the fluorescence (singlet to singlet) and phosphorescence (singlet to triplet) paths. Yet, the S_2 decay rate for the process is extremely fast ($50\ fs$) [10]. These phenomena led to the conclusion that the relaxation takes place through internal conversion (IC). Ref. [11] measured the spectrum for the internal vibrational relaxation which takes place immediately after the IC process and found bands which belong to the $C-H$ stretching bonds, i.e. around $3000cm^{-1}$. While other accepting modes are not excluded, (for example, no data was given as to the region around $1600cm^{-1}$), this gives a clear indication that a significant amount of the electronic energy is transferred in the relaxation process to the $C-H$ modes.

In benzene the electronic state change between the ground state and the first excited states is concentrated on the $C-C$ aromatic ring system. Therefore, the $C-C$ modes are the most displaced relative to the ground electronic state. From a classical point of view, it is easy to show that in the general case, the mode that is the most displaced is the mode that receives the energy. The experimental results mentioned above stands as one of the counter examples for this classical behavior. We use here the phase-space analysis to show that this result can be easily explained.

To set the groundwork for the analysis in the next sections, we first review what is known (and unknown) about the modes of vibration and the electronic surfaces involved in the process.

A. The S_0 surface potential

The configuration of the ground S_0 electronic state of the benzene is hexagonal and belongs to the D_{6h} symmetry group. The benzene molecule has $3N-6=30$ modes of vibrations. In the normal mode coordinates 20 of these modes belong to 10 degenerate pairs. A displacement of a normal mode in an equilibrium configuration cannot take place unless the mode is totally symmetric. For the benzene molecule in the D_{6h} symmetry only two normal modes of vibration belong to the totally symmetric, a_{1g}, representation: the totally symmetric stretching of the $C-C$ bonds (q_1) and $C-H$ bonds (q_2). (The numbering of the modes in this paper is done according to Wilson [19]). We mention here the normal modes which have special importance in the rest of the paper. The six in plane $C-H$ stretching normal modes are six orthogonal linear combinations of the six local $C-H$ in-plane stretching modes s_i and can be displayed by the 6×6 unitary matrix transformation:

$$\begin{pmatrix} q_2\,(a_{1g}) \\ q_7\,(e_{2g}) \\ q_{13}\,(b_{1u}) \\ q_{20}\,(e_{1u}) \\ q_{7a}\,(e_{2g}) \\ q_{20a}\,(e_{1u}) \end{pmatrix} = \frac{1}{\sqrt{6}} \begin{pmatrix} 1 & 1 & 1 & 1 & 1 & 1 \\ \sqrt{2} & -\frac{1}{\sqrt{2}} & -\frac{1}{\sqrt{2}} & \sqrt{2} & -\frac{1}{\sqrt{2}} & -\frac{1}{\sqrt{2}} \\ 1 & -1 & 1 & -1 & 1 & -1 \\ \sqrt{2} & \frac{1}{\sqrt{2}} & -\frac{1}{\sqrt{2}} & -\sqrt{2} & -\frac{1}{\sqrt{2}} & +\frac{1}{\sqrt{2}} \\ 0 & \frac{\sqrt{6}}{2} & -\frac{\sqrt{6}}{2} & 0 & \frac{\sqrt{6}}{2} & -\frac{\sqrt{6}}{2} \\ 0 & \frac{\sqrt{6}}{2} & \frac{\sqrt{6}}{2} & 0 & -\frac{\sqrt{6}}{2} & -\frac{\sqrt{6}}{2} \end{pmatrix} \begin{pmatrix} s_1 \\ s_2 \\ s_3 \\ s_4 \\ s_5 \\ s_6 \end{pmatrix} \tag{21}$$

Figure 3 displays a physical picture of the $C-H$ stretching modes.

An enormous amount of work was done by quantum chemists to find the electronic S_0 surface potential of the benzene. The most recent paper that gives *ab-initio* results for S_0 is by Miani et al. [20] . We take the form of the ground-state potential energy surface from [21] to be:

$$V(\vec{q}) = \frac{1}{2}\sum_{k=1,2} m_k\,(\omega_k^g)^2\,(q_k - q_k^g)^2 + \frac{1}{6}\sum_{ijk=1,2}\phi_{ijk} r_i r_j r_k + O(q^4)\ , \tag{22}$$

where:

$$r_i = \sqrt{\omega_i^g m_i}(q_i - q_i^g) \tag{23}$$

Here $\omega_k^g = \tilde{\omega}_k^g[cm^{-1}]\,/\,2R_\infty$, $q_k^g = \tilde{q}_k^g[cm]\,/\,a_0$, and $m_k = \tilde{m}_k\,/\,m_e$, are the frequencies, displacements, and reduced mass of the modes in a.u., where R_∞, a_0, and m_e are Rydberg constant, the Bohr radius, and the electron mass of the ground electronic state respectively. From here on we use the parameters in the a.u. scale. The anharmonic force field constants $\phi_{ijk} = \tilde{\phi}_{ijk}[cm^{-1}]\,/\,2R_\infty$ are taken from [20]. As mentioned above the only modes with non-zero equilibrium position at the S_0 hexagonal conformation are $q_1^g = 6.47$ Bohrs and $q_2^g = 5.02$ Bohrs.

B. The S_2 surface potential

Much less is known about the S_2 surface potential. The known values used in this paper are

the harmonic frequencies calculated by [22]. The anharmonicities and the displacements of the S_2 potential surface are not known. The symmetry group of S_2 can be D_{6h}, as in S_0, or D_{2h} due to a pseudo-Jahn-Teller effect [7]. The normal modes of vibration may be the same as in S_0 or different, due to a possible Duschinsky mode rotation, i.e. coupling of non-degenerate modes that belong to the same symmetry representation. In section IV we use the simplest ansatz for these unknown properties. We neglect the anharmonicity of S_2 , assume a D_{6h} symmetry, no Duschinsky effects, and displacements as in the S_1 state, $q_1^g = 6.63$ Bohrs and $q_2^g = 5.01$ Bohrs [7]. This over-simplified model is needed in order to understand the mechanism of the transition, and it forms the reference frame for more realistic models considered in section 5. In section 5.1 we treat the displacements as free parameters. In section 5.2 we consider anharmonic effects on the S_2 state. In section 5.3 we assume a D_{2h} symmetry and in section 5.4 we consider one possible Doschinsky mode rotation which mixes between q_{14} and q_{15}.

IV. SURFACE JUMPING IN BENZENE

In this section we use only known parameters and the simplest possible conjectures for the unknown parameters. In the next section we consider the possible impact of the different unknown parameters.

A. The initial Wigner function

For the sake of simplicity, we consider the non radiative transition from the vibrationless state of the S_2 to the manifold quasi-continuum states of the $S_0(A_{1g})$ ground electronic state. Relaxation from higher vibrational states can be considered in a similar way.

Taking the initial state of S_2 to be the ground state wave function for the normal mode k of a harmonic oscillator we have:

$$\phi_I^k(q_k) = \left(\frac{m_k\omega_k^e}{\pi\hbar}\right)^{1/4} \exp\left[-\frac{1}{2}\frac{m_k\omega_k^e}{\hbar}(q_k - q_k^e)^2\right] , \tag{24}$$

where ω_k^e and q_k^e are the frequency and the equilibrium configuration of the k normal mode of the e excited electronic state, respectively. For S_2, $e = 2$. The total wave function is a product of the wave functions of each of the modes. The Wigner transform of a gaussian wave function is another gaussian, for mode k :

$$\rho_I^k(q_k, p_k) = \frac{1}{\pi\hbar} \exp\left[-\frac{m_k\omega_k^e}{\hbar}(q_k - q_k^e)^2 - \frac{p_k^2}{m_k\omega_k^e\hbar}\right] . \tag{25}$$

The initial total Wigner function is:

$$\rho_I(q,p) = \prod_{k=1}^{30} \rho_I^k(q_k, p_k) \equiv \left(\frac{1}{\pi\hbar}\right)^{30} e^{-W}. \tag{26}$$

The $S_2 \to S_0$ IC is a forbidden transition. Therefore, when calculating the transition rates or the jumping point, the initial Wigner function $\rho_I(q,p)$ should be replaced by $\rho_I^{(\mathsf{p})\prime}(q,p)$ as defined and explained in section 2.2. Taking ϕ_I^{p} to be as in Eq. (24) we get:

$$\rho_I^{(\mathsf{p})\prime}(q,p) = \frac{m_{\mathsf{p}}\omega_{\mathsf{p}}^e}{\hbar}\left(\frac{m_{\mathsf{p}}\omega_{\mathsf{p}}^e}{\hbar}(q_{\mathsf{p}} - q_{\mathsf{p}}^e)^2 + \frac{p_{\mathsf{p}}^2}{m_{\mathsf{p}}\omega_{\mathsf{p}}^e\hbar}\right)\rho_I(q,p). \tag{27}$$

The integral over the nuclear degrees of freedom giving the transition strength for a forbidden transition differs from the FC factor squared for an allowed transition by an additional polynomial in the integrand multiplying the Gaussian initial Wigner function. With this additional factor, the transition probability would vanish for a zero excitation of the promoting mode and therefore the promoting mode must have, at least, some minimal excitation.

The jumping point for an allowed transition is found by maximizing $\rho_I(q,p)$ while the jumping point for a forbidden transition is found by maximizing $\rho_I^{\prime(\mathsf{p})}(q,p)$, both under the same constraint: $H_F(q,p) = E$. It can be shown that when surface jumping occurs these two procedures give the same quantum jump. For large excitations of the promoting mode, the behavior of the Wigner function is dominated by the exponent and the influence of the polynomial is negligible. For small excitations of the promoting mode there is, as mentioned above, a minimal amount of energy that must be transferred to the promoting mode of vibration yet this hardly affects the quantum jump. Thus, we maximize $\rho_I(q,p)$ and not $\rho_I^{(\mathsf{p})\prime}(q,p)$.

Within the harmonic approximation ρ_I is a gaussian and minimization of the argument in the exponent W is equivalent to the maximization of ρ_I. Therefore, we look for minima of W defined in Eq. (26) under the constraint $H_F(q,p) = E$. We analyze the system in two steps: first by using

a harmonic approximation for H_F and second by including the anharmonic force field of Ref. [20]. For convenience we use, at first, normal modes coordinates.

B. Harmonic ground electronic potential

Consider a harmonic approximation for the Hamiltonian of the lower electronic surface:

$$H_F^h = \frac{1}{2}\sum_{k=1}^{30}\left[\frac{p_k^2}{m_k} + m_k\left(\omega_k^g\right)^2\left(q_k - q_k^g\right)^2\right] \quad . \quad (28)$$

Results of our calculations show that the extremum points (q^*, p^*) of W under the constraint $H_F^h = E$ form an 11 dimensional subspace within the 60-dimensional phase space of the problem. All of the points in this subspace include a small position excitation of the $C-C$ totally symmetric mode (around 2% of the total energy) and an arbitrary position or momentum excitation of the six $C-H$ in plane stretching modes. The Wigner function $\rho_I(q,p)$ is highly peaked on this subspace with all the points having the same value of the (argument of the) Wigner function, which is our measure of the level of propensity for a transition at these points, $W \cong 32$. A closed-form solution for the harmonic approximation can be found in Ref. [5] for the case of displacement in only one direction and in Ref. [17] for a general displacement. For our system the analytic solution confirms the numerical results. Second inspection of the $C-H$ normal modes with the same high propensity show that they have almost the same value of $m_i\omega_i^2$ and could be considered as degenerate oscillators. We conclude that:

- Within a harmonic approximation the surface jumping is restricted to an 11-dimensional hypersurface within the 60-dimensional phase-space of the problem. The surface, with $W \cong 32$, represents all the combinations of in-plane $C-H$ stretching modes subject to the demand of energy conservation.

C. Anharmonic ground electronic potential

In this subsection we repeat the analysis of the previous subsection with the same initial harmonic state on the excited electronic surface but this time with the most recent anharmonic force field for the ground state potential surface:

$$H_F = \frac{1}{2}\sum_{k=1}^{30}\left[\frac{p_k^2}{m_k} + m_k\left(\omega_k^g\right)^2\left(q_k - q_k^g\right)^2\right] + \frac{1}{6}\sum_{ijk}\phi_{ijk}r_i r_j r_k \ . \quad (29)$$

Although adding the anharmonic force field in this asymmetric fashion does not seem self consistent, we do so first, and then, in the next section, we check the possible effects of anharmonicities of the excited surface. Accurate anharmonic force field for the (second) excited state is not available to our knowledge and the enormous number of anharmonicity constants can not be simply treated as free parameters.

In table 1 we show the points found by the numerical minimization of W under the constraint $H_F = E$. The points which have the lowest value of W, highest propensity, have an almost sixfold degeneracy with $W \cong 17$. These points correspond to the same small position excitation of the totally symmetric $C-C$ stretching mode and different specific combinations of the six $C-H$ stretching modes position excitations.

The data in the literature led us to perform the analysis in the normal modes of vibrations framework, yet, in order to decode the meaning of the points we have transformed the coordinates from normal modes to local modes using the inverse matrix of the transformation (21). In table 2 we present the same points as in table 1 in local mode coordinates. The physical meaning of the points is now obvious. The six points with the highest propensity refer to six equal points of local mode excitation of $C-H$ stretching with an addition of a very small excitation of the totally symmetric $C-C$ stretching mode which is the only significantly displaced mode within the 30 modes of the benzene.

D. Local vs. normal coordinates

The best choice of coordinates for the description of molecular spectroscopy depends on the exact process that has to be described. Low energy vibrational excitations like IR absorption spectroscopy are usually described in terms of normal modes oscillators while high energy processes like dissociation are best described within a local mode framework. It is clear that dissociation of a molecule occurs by breaking one local mode between two atoms; this is inconveniently described by high excitation of several bonds between atoms in the normal mode description.

In our analysis the excitation of a local $C-H$ mode seems to have its origin in the structure of

the surface potential. Using the local coordinates, the surface potential for the six in plane $C-H$ stretching modes has the form:

$$V = \sum_{i,j} V_{ij} s_i s_j + \sum_{i,j,k} V_{ijk} s_i s_j s_k \,. \qquad (30)$$

Because of the symmetry of the problem $V_{11} = V_{22} = V_{ii}$, $V_{12} = V_{23} = V_{34} = V_{i,i+1}$ etc.. The use of this form reduces the number of parameters that determine the third order anharmonic surface potential to only twelve parameters (instead of 56 in the general normal description). This fact may encourage the attempt to represent the surface potential we took from [20] in local modes. After this transformation of the coordinates we have found that all the cross coefficients in the local modes formulation are very close to zero. We thus find that the potential represents six *separable* anharmonic oscillators. This reduces the number of parameters that describe the anharmonic potential to only *two*. The separability of the potential leads to a straightforward understanding of the reason for a local excitation found in our calculations. It can be proven that in this case of separate potentials with cubic anharmonicity the point with highest propensity corresponds to a single local excitation [6,17]. We must note here also that the possibility of diagonalizing the potential in local modes was suggested already 30 years ago in order to understand the overtones of the $C-H$ in plane stretching in the IR spectrum of the benzene [23,24]. Here we started with normal modes but are forced by the results of our calculation to change to local modes.

We summarize our conclusions so far:

- Inclusion of anharmonic effects for the ground electronic state reduces the dimensionality of the transition from an 11 dimensional hyperspace to small regions surrounding six degenerate points.
- The points with the highest propensity describe a single excitation of a local mode of $C-H$ stretching and another considerably smaller simultaneous excitation of the totally symmetric $C-C$ stretching mode.

V. SENSITIVITY TO DIFFERENT CONJECTURES REGARDING THE S_2 SURFACE POTENTIAL

As mentioned in section III, a lot of information regarding the S_2 surface potential is unknown. In this section we (separately) treat many of the missing parameters as free parameters and check the sensitivity of the results obtained in the previous section to these changes.

The following subsections consider:

1. Different displacements of the S_2 surface (with no change of the symmetry of the molecule).
2. Anharmonicity of the upper surface (within the assumption of seperability).
3. Different symmetry of the S_2 surface (D_{2h} instead of D_{6h}) due to a possible pseudo-Jahn-Teller effect.
4. A possible Duschinsky mode rotation.

A. Displacements of the S_2 surface potential

The actual $C-H$ and $C-C$ bond lengths of the S_2 state are, to our knowledge, unknowns. Moreover, the actual conformation of the molecule in the S_2 state is in doubt. In this subsection we assume that the symmetry of the benzene is conserved in the S_2, i.e. the molecule is hexagonal and belongs to the D_{6h} point group of symmetry. Therefore, the only modes that can have non-zero displacements are the totally symmetric $C-H$ and $C-C$ breathing modes. We take the potentials from section 4.2, implement our maximization procedure and search for jumping points for different displacements of $q_1(C-C)$ and $q_2(C-H)$.

Figure 4 displays the non-zero coordinates of the jumping point with the highest propensity and the value of the Wigner function at this point, versus the displacement of the $C-C$ bond length. From the graph it is easy to see that the main change of the excitation is in the $C-C$ totally symmetric direction. The dependence is linear with a slope of almost 1.1, (see Ref. [17] for an analytic derivation of a similar result in the harmonic case). Changes of the $C-H$ local excitation and of the value of the Wigner function at the jumping point, are small and nonlinear.

In figure 5 we display the coordinate of the jumping point with the highest propensity and the value of the Wigner function at this point, versus the displacement of the $C-H$ bond length. Again, the excitation of the displaced mode, here the totally symmetric $C-H$ stretching *normal* mode, is linearly proportional to the displacement (as in a vertical transition). The totally symmetric $C-C$ is not affected at all, while the local $C-H$ stretching mode which is the mode that

undergoes the jump is again slightly, nonlinearly, affected. Note that in this framework the normal and local $C-H$ stretching act like almost different directions in space.

The picture is of one mode undergoing a jump while an almost vertical transition takes place for the other modes. This is demonstrated in figure 7 which plots the excitations in the different directions and the value of the Wigner function at the jumping point for different energy gaps between the states with fixed displacements between the modes. The only mode which changes its excitation due to the change of the energy gap is the mode which undergoes the jump, here - local $C-H$ stretching. The other modes undergo an almost vertical transition and do not show any change of the excitation with the change of the energy that goes into the vibrational degrees of freedom. The value of ρ $(= e^{-W})$ decreases with the increase of the energy gap between the surfaces. This feature is ascribed to the fact the enlargement of the gap between the surfaces leads to a larger quantum jump between them, a process which is classically forbidden and therefore less probable.

- When one direction in phase-space dominates the quantum jump, excitations in other directions are proportional to the displacement, as if in a vertical transition.

B. Anharmonicities for the S_2 potential surface

In the previous section we showed the separability in the subspace of $C-H$ stretching modes of the ground surface potential. Full treatment of the anharmonicities of the high electronic surface as free parameters without assuming separability is a formidable task and is not considered here. Here, we assume separability and study the influence of the anharmonicity of the upper surface on the jumping point within the effective one dimensional problem.

Figure 7 displays the one dimensional ground and excited electronic surface potentials in the local mode representation. Relative to the harmonic potential which is, of course, symmetric, the anharmonic potential is softened on its dissociation part and has a sharper slope on its close approach part. Applying a harmonic approximation for both surfaces gives the value of the Wigner function at the jumping point of $W \cong 32$. Taking the ground surface potential to be anharmonic gives the value of $W \cong 17$. Taking into account the anharmonicities of the excited state makes both the wave function and the Wigner function wider on the dissociation side of the potential and narrower on the close approach side. Consequently, the value of the Wigner function at the jumping point $W(q^*, p^*)$ gets a value between the two extremes of $32 \leq W \leq 17$.

For a quantitative analysis of this property and in order to make the calculation with an anharmonic potential that has a closed form expression for the initial Wigner function, we use a Morse approximation for the excited potential surface:

$$V_e(q) = D\left[1 - e^{-\beta(q-q_0)}\right]^2 \tag{31}$$

where: $\beta = \sqrt{2m\omega x_e / \hbar}$ and ω, m, x_e, and $D = \hbar\omega / 4\, x_e$, are the harmonic oscillator frequency, the reduced mass of the mode, the anharmonicity, and the dissociation energy of the excited electronic state. The dissociation energy for the ground electronic state is $D_g = 110.9\,\mathrm{kcal/mol} = 0.1701\,\mathrm{Hartree}$ [25]. Some experimental data, like the acidity of the benzene molecule on the excited electronic state [26], indicate to a difference of less then 10% between the dissociation energy of the excited and ground states. The dashed line in figure 7 is the Morse potential for the above values. From the graph it is obvious that the high order Taylor series anharmonic force field and the Morse potential approximations are very distinct approximations. We prefer therefore to use in this subsection Morse potential for both the ground and excited states.

The wave function of the Morse oscillator is a combination of the associated Laguerre polynomials and the Wigner function is a combination of the modified spherical Bessel function of the third kind (MacDonald function) [27,28]. The Wigner function of the ground vibrational state is:

$$\rho(q,p) = \frac{2}{\pi\hbar}\,\frac{x_e^{-2}}{\Gamma(1/x_e - 1)}\, e^{-2\beta(q-q_0)}\, K_{-2ip/\beta\hbar}\left(x_e^{-1}\, e^{-\beta(q-q_0)}\right), \tag{32}$$

where Γ is the Γ function. The order of the MacDonald function that we study is zero because the momentum at the jumping point is zero, $p^* = 0$, and we study $\rho(q, p^*)$. Figure 8b displays some examples of Wigner functions, (with $p = 0$), for the same frequency ω but different anharmonicities x_e. The function is a slightly deformed gaussian where the close approach side of the function decays more rapidly with the increase of the anharmonicity. Figure 8a displays the projection of the jumping point with the highest propensity on

the various modes and the value of the Wigner function at this point, versus the anharmonicity parameter x_e of the upper surface, keeping the anharmonicity of the lower surface fixed. The main feature of the graph is the decrease of the value of the Wigner function at the jumping point with the increase of this anharmonicity. The increase of the anharmonicity makes the closed-approach side of the Wigner function narrower. This side is the one on which the jump between the surfaces takes place and therefore the sharpening of the function on this side decreases the value of the Wigner function at the jumping point. The values for W are within the qualitative predicted range discussed above. The only apparent (although small) change of the jumping point with the change of x_e is on the $C-H$ totally symmetric normal mode axis. The deformation of the Wigner function due to the anharmonicity x_e moves the center of the initial wave packet to the dissociation side of the potential. This change of the center of the wave packet leads to an effective positive displacement of the wave packet and the center of the wave packet on the ground electronic surface undergoes an almost vertical transition to a point in space which is displaced with respect to the ground configuration, *although there is no real displacement between the two surfaces.*

Another interesting feature that arises from the reduction of the problem to one dimensional Morse potential regards the direction of the sudden change in the local $C-H$ stretch. The dissociation energy of the S_0 state is $0.117eV$, while the vertical gap between S_2 and S_0 is $0.228eV$. Therefore, a jumping point on the dissociation side has to include a transfer of the energy to momentum excitation. However, for momentum excitation, which is always harmonic, we already made the analysis and found a very low propensity of $W \cong 32$. The jumping point is predominantly on the close approach side of the potential. One may conclude that the wave packet lands on the ground electronic surface at the close approach side of the potential and that the molecule has time to decay vibrationally before it can dissociate.

- An increase of the Wigner function at the jumping point is obtained with an increase of the anharmonicity of the lower surface.
- For a fixed anharmonicity of the lower surface, a decrease of the Wigner function at the jumping point is obtained with an increase of the anharmonicity of the upper surface.
- The anharmonicity on the upper surface gives correction to the two extreme approximations of harmonic-harmonic and anharmonic-harmonic potentials.
- Anharmonicity can induce small excitation of non displaced modes due to changes in the center of the initial wavepacket.

C. Pseudo-Jahn-Teller effect

Several papers had claimed that the D_{6h} symmetry of the S_2 of the benzene molecule is distorted to D_{2h}. Lowering the symmetry of the excited state can lead to addition of normal modes which belong to the totally symmetric representation. Such modes can have non-zero equilibrium displacements on the upper deformed surface. Within the 28 non totally symmetric modes for the hexagonal benzene with a D_{6h} symmetry group only four modes become totally symmetric to the lower D_{2h} symmetry. In the D_{6h} symmetry these modes belong to the degenerate e_{2g} representation which splits into two non-degenerate representations of the D_{2h} symmetry, one of which is the a_g totally symmetric representation. Two of the four modes relate to changes of $C-H$ conformation (q_7 and q_9) whereas the other two (q_6 and q_8) refer to changes of $C-C$ conformation. To very good accuracy it can be assumed that the significant change on the molecule conformation takes place on the ring and not in the $C-H$ bonds. Thus, the main changes of the displacements would be for the q_6 and q_8 normal modes. Diagrams of these two modes are given in figure 9.

We must note here also that in general, a significant change of the force field of the potential can take place and tremendously change the harmonic and non-harmonic coefficients. Here we assume, as in Ref. [22], that for the benzene the main influence of a pJT distortion of the excited S_2 state potential, if exists, is due to a non-zero displacements of the two modes q_6 and q_8 of in-plane vibrations of the ring. This may change the coordinates of the jumping point but not its zero momenta. The possibility of an extreme change also in the frequency of these modes will be studied elsewhere. Remarkable changes of the frequencies of q_6 and q_8 (mostly in the triplet state but maybe also in the singlet) were considered for example in Refs. [29,30].

The results of the calculations are given in figures 10 and 11. In figure 10 we display the nonzero coordinates of the jumping point with the highest

propensity and the value of the Wigner function at this point versus the difference between the angles of the benzene ring. Difference between the angles gives a nonzero displacement of q_6. Again, we see that the excitation of a displaced mode, here q_6, linearly depends on the displacement. Excitations of the other modes do not significantly change. Figure 11 plots the coordinates of the jumping point with the highest propensity and the value of the Wigner function at this point versus the difference between the $C-C$ bond lengths. This change of the bond lengths induces displacements in q_8 and q_1 and as a result a change in the coordinates of the jumping point.

Even for a moderate change in the symmetry a noticeable amount of the energy is transferred to modes that are displaced due to the pJT effect. This may be used as an experimental way to measure, qualitatively at least, the existence of the pseudo-JT effect in the S_2 excited electronic state. The effect would manifest itself as additional IR peaks in the vibrational relaxation spectrum of the S_0 electronic state following the $S_2 \rightarrow S_0$ internal conversion.

- For moderate pJT deformations we can expect additional features in the IR vibrational relaxation spectrum of the benzene molecule. This can be ascribed to changes in the transition point proportional to the displacement of modes on the excited surface.

D. Duschinsky rotation

Consider the impact of a possible Duschinsky rotation which couples q_{14} and q_{15}. Figure 12 displays diagrams of these two modes as they appear on the ground electronic state. The new normal modes on the excited state are mixed according to:

$$\begin{pmatrix} q'_{14} \\ q'_{15} \end{pmatrix} = \begin{pmatrix} \cos\beta & \sin\beta \\ -\sin\beta & \cos\beta \end{pmatrix} \begin{pmatrix} q_{14} \\ q_{15} \end{pmatrix} \qquad (33)$$

where β is the angle of rotation between the axis. According to Ref. [31], these two modes are coupled in this way on the first excited electronic surface. Here, we consider such a possible coupling for the second excited surface. Other conjectures for other mixing can be studied in a similar way.

The rotation in two dimensions and its influence on the jumping point is demonstrated in figure 13. The contours of the initial Wigner function on the excited electronic surface and the constraint on the lower surface $H_F = E$ are plotted by solid and dashed lines, respectively. The implementation of the Duschinsky rotation is done by rotating the inner ellipse by the angle β. A larger difference between the widths of the Wigner function would increase the effect of the rotation. The effect has to be considered in position as well as in momentum space. However, in our calculations no momentum excitation is found. We first examine the case $\beta = 90^0$, i.e. $q'_{14} = q_{15}$ and $q'_{15} = -q_{14}$ and find a new couple of points with high propensity with a large excitation of q_{14} and small excitations of the totally symmetric $C-C$ and $C-H$ stretching q_1 and q_2. The value of W at these points is 16.8, very close to the value of the points with the highest propensity found without the Duschinsky rotation. The new point that we have found for the extreme rotation is used as an initial point for a local minimum search for different angles of rotation. In figure 14 we display this local minimum which is found in our calculations and the value of the Wigner function at this point versus β, the rotation angle.

A new jumping point with significant propensity develops only for angles of rotation above 65^o. For smaller rotations the point that originates from a rotation exists as a local minimum but has a very high value of W which makes the probability of decaying through this channel negligible.

The importance of the absolute value of the frequency and the reduced mass of a mode in the determination of its propensity as an accepting mode was previously discussed [32,33] with implications for the isotope effect for nonradiative decay [33].

- Duschinsky effect can cause, in general, a change of the direction of the quantum jump but for the benzene molecule the angles for rotation needed for this feature to appear are non-physical.

VI. SUMMARY AND CONCLUSIONS

The surface jumping method for nonvertical transitions was applied to recognizing accepting modes in a model of the $S_2 \rightarrow S_0$ transition in benzene. In order to do so, we had to extend the formalism to forbidden transitions. This results in an additional factor in the FC integrand, a polynomial of the position and momentum of the promoting mode of vibration. Surface jumping may involve an excitation of only one mode of the system, which takes most of the energy, or it may involve many modes in a concerted jump. Here we found that the C-H modes undergo the

jump, as had been surmised through the years by a variety of experimental and theoretical clues.

We showed that jump takes place in the *local* C-H modes: Since the energy gap between the states is large compared to the vibrational energy scale and the ratio of the harmonic frequencies between the surfaces does not differ very much from one ($0.7 < \omega_k^e \,/\, \omega_k^g < 1.2$), the modes with the largest frequency and smallest reduced mass are the modes that undergo the jump. The *local* $C-H$ in-plane stretching modes take almost all of the electronic energy. (If a strong pseudo-Jahn-Teller effect exists, it seems that the energy will be divided between the local $C-H$ stretching modes and the q_8 and q_6 normal modes depicted in figure 9.)

Treating the displacements of the totally symmetric modes of the benzene (under the assumption of hexagonal configuration for the excited state) as free parameters we found that the excitation of a displaced mode is proportional to its displacement. The system decays by one jump to a favorable direction while all the other directions undergo a transition which is almost vertical.

We examined the sensitivity of the method to different conjectures regarding the unknown parameters of the excited S_2 electronic potential, including the impact of a possible pseudo-Jahn-Teller effect on the excited surface and suggested a possible qualitative detection of pseudo-Jahn-Teller and Jahn-Teller effects on electronic states by checking the IR spectrum that follows the IC from a pJT or JT deformed state. We have also checked the possible influences of a Duschinsky mode rotation and concluded that such a rotation could lead, in some cases, to an opening of a decay channel which is negligible without the Duschinsky rotation. The impact increases with the difference between the oscillator strengths of the two modes which mix due to the rotation. However, in our case of the $S_2 \rightarrow S_0$ IC of the benzene molecule we found the angle of rotation that would make a noticeable effect to be non-physical. For the transition considered here, the influence of the polynomial term on the direction of the jump can be neglected. More generally, the maximization procedure with this additional term is mathematically equivalent to the consideration of a decay not from the ground vibrational state but from a vibrationally excited state.

Some of the issues to be considered in the future include a mathematical analysis of different analytic models [17], transitions from thermal distributions [34], rotations, and an implementation of the method to other molecules. Application to dissociation, the coupling of the vibrational space of the molecule to additional degrees of freedom of a medium, the dynamics of the molecular wavepacket after the quantum jump between the surfaces takes place, and the calculation of the rate using the phase-space method, could also be studied within this approach. Decay from an excited state and the influence of the promoting mode, i.e. the role of polynomial factors in the FC integrand deserves further study. Isotope effects and the competition between the accepting modes, for example local $C-H$ and normal q_8 and q_6 also deserve farther study.

ACKNOWLEDGMENTS

B.S. gratefully acknowledges useful discussions with Prof. Benjamin Scharf. This research was supported by Grant No. 9800460 from the United States - Israel Binational Science Foundation (BSF), Jerusalem, Israel.

[1] R.K. Preston, and J. C. Tully, J. Chem. Phys. **54**, 4297 (1971).

[2] L.D. Landau and E.M. Lifshitz, *Quantum Mechanics* (Pergamon, London, 1958), chapter 7.

[3] E.S. Medvedev, Chem. Phys. **73,** 243 (1994).

[4] E.S. Medvedev, J. Chem. Phys. **100,** 2027 (1994).

[5] B. Segev and E.J. Heller, J. Chem. Phys. **112**, 4004 (2000).

[6] E.J. Heller and D. Beck, Chem. Phys. Lett. **202**, 350 (1993).

[7] L.D. Ziegler and B.S. Hudson, Excited States **5**, 41 (1982).

[8] C.S. Parmenter and M.W. Schuyler, Chem. Phys. Lett. **6**, 339 (1970).

[9] E. Sekreta and J.P. Reilly, Chem Phys Lett. **149**, 482 (1988).

[10] W. Radloff, V. Stert, T. Freudenberg, I.V. Hertel, C. Jouvet, C. Dedonder-Lardeux, and D. Solgadi, Chem. Phys. Lett. **281**, 20 (1997).

[11] J. Shan, M. Suto, and L.C. Lee, J. Photoch. Photobio. A **63**, 139 (1992).

[12] E. J. Heller, J. Chem. Phys. **68**, 2066 (1978).

[13] E. J. Heller and R. C. Brown, J. Chem. Phys. **79**, 2226 (1983).

[14] B. Hüpper and B. Eckhardt, Phys. Rev. A. **57**, 1536 (1998).

[15] B. Hüpper and B. Eckhardt, J. Chem. Phys. **110,** 11749 (1999).

[16] The small parameter for the expansion is $s = \left[\hbar/\sqrt{2m\,|\nabla V|}\right]^{2/3}/\sigma$. In [15] $s \approx 0.6$ was small enough to assure convergence. Here, the Gaussian on the excited surface has a width of $\sigma = \sqrt{\hbar/m_k\omega_k^e} \approx 0.2$ while the gradient of the ground potential surface at the jumping point is $|V'(q^*)| \approx 1$, $m \approx 2000$, and $s \approx 0.3$. In [15] higher order terms were also calculated, yet this was within a calculation for the rate. Here we calculate propensities, which are controlled by the leading order term in the expansion.

[17] A. Sergeev, B. Segev, S. Kallush and E.J. Heller, unpublished.

[18] W. H. Press *et al.*, *Numerical Recipes* (Cambridge University Press, Cambridge, 1986) p. 635.

[19] E.B. Wilson Jr, J.C. Decius, and P.C. Cross, *Molecular Vibrations and theory of Infrared and Raman Vibrational Spectra* (McGraw-Hill Book Company, New York, 1955), Chapter 10.

[20] A. Miani, E. Cane, P. Palmieri, A. Trombetti, and N.C. Handy, J. Chem. Phys. **112**, 248 (2000).

[21] D. Papoused and M.R. Aliev, *Molecular Vibrational-Rotational Spectra* (Elsevier, Amsterdam, 1982), chapter 23.

[22] R.J. Sension, R.J. Brudzynsky, S. Li, and B.S. Hudson, J. Chem. Phys. **96**, 2617 (1992).

[23] B.R. Henry and W. Siebrand, J. Chem. Phys. **49**, 5369 (1968).

[24] See also: L. Halonen, Chem. Phys. Lett. **87**, 221 (1982), and references therein.

[25] *Handbook of Physical and Chemistry Constants,* edited by S.P. Clarl, Jr. (Spriger, Berlin, 1990).

[26] J.F. Ireland and P.A.H. Wyatt, Adv. Phys. Org. Chem. **12**, 131 (1976).

[27] H.W. Lee, Phys Rep. **259**, 147 (1995).

[28] A. Frank, A.L. Rivera, and K.B. Wolf, Phys. Rev. A **61** , 4102 (2000).

[29] B. Scharf, Chem. Phys. Lett. **68**, 242 (1979).

[30] W.J. Buma, J.H. van der Waals, and M.C. van Hemert, J. Chem. Phys. **93**, 3733 (1990).

[31] G. Fischer, *Vibronic Coupling* (Academic Press, London, 1984).

[32] R. Englman, *The Jahn-Teller Effect in Molecules and Crystals* (Wiley Interscience, London-New York, 1972); *Non-Radiative Decay of Ions and Molecules in Solids* (North Holand Pub. Co., Amsterdam, 1979).

[33] J. Jortner, S.A. Rice and R.M. Hochstrasser, Adv. Photochem. **7**, 149 (1969).

[34] Y. Japha and B. Segev, unpublished.

q_1	q_2	q_7	q_{13}	q_{20}	q_{7a}	q_{20a}	W
0.08	-0.31	-0.44	-0.31	-0.44	0	0	17.00
0.08	-0.31	-0.44	0.31	0.44	0	0	17.00
0.08	-0.32	0.22	0.31	-0.22	-0.38	-0.38	17.02
0.08	-0.32	0.22	-0.31	0.22	-0.38	0.38	17.02
0.08	-0.32	0.22	-0.31	0.22	0.38	-0.38	17.02
0.08	-0.32	0.22	0.31	-0.22	0.38	0.38	17.02

TABLE I. Local maximum or jumping points obtained for the $S_2 \rightarrow S_0$ transition using the potential of section 4.3. The points are given in the normal mode representation

s_1	s_2	s_3	s_4	s_5	s_6	W
-0.76	0.	0.	0.	0.	0.	17.00
0.	0.	0.	-0.76	0.	0.	17.00
0.	-0.76	0.	0.	0.	0.	17.02
0.	0.	-0.76	0.	0.	0.	17.02
0.	0.	0.	0.	-0.76	0.	17.02
0.	0.	0.	0.	0.	-0.76	17.02

TABLE II. The points of table 1 in the local mode representation.

FIG. 1. Two kinds of transitions: vertical and non-vertical. (a) Radiationless vertical transition between crossing surfaces. The transition takes place by continuous changes of the coordinates and via the point of crossing between the surfaces. (b) Radiationless non-vertical transition for nested surfaces - surface jumping. The transfer of the energy must occur by a sudden change of position or momentum. The direction of the jump is not obvious a priory. Our purpose is to predict this direction. (c) Radiative vertical transition, equivalent to the radiationless case (a): most of the energy goes to the emitted photon. The transition takes place by continuous changes of the coordinates and via the point of crossing between the dressed initial surface and the final accepting energy surface. (d) Radiative non-vertical transition, equivalent to the radiationless case (b): such transitions occur in the blue wing of an absorption band, where some of the energy of the absorbed photon is transferred into vibrational energy via surface jumping.

FIG. 2. Geometric representation of the method for finding the direction of the quantum jump in two dimensions (Q_1, Q_2). The outer dashed ellipse represents the constraint $H_F(Q_1, Q_2) = E$. The inner solid ellipses represents the contours of the Wigner function on the upper surface. (a) The case of strong maximum. The value of the Wigner function decreases rapidly with the distance from the jumping point. The jumping point is well defined. (b) Weak maximum - the jumping point is not well defined.

FIG. 3. The $C - H$ in-plane stretching normal modes. q_2 $(a_{1g})$and $q_{13}(b_{1u})$ are two non-degenerate modes. q_2 is the totally symmetric $C - H$ stretching. $q_7(e_{2g})$ and $q_{20}(e_{1u})$ are two degenerate modes.

FIG. 4. Results of the calculation for the $S_2 \rightarrow S_0$ transition taking the potentials of section 4.3 with the displacement of the $C - C$ totally symmetric mode considered as a free parameter. The coordinates and the value of the Wigner function at the jumping point are plotted vs. the $C - C$ displacement between the two surfaces. The excitations of the local $C - H$ and totally symmetric $C - C$ stretching and the value of the Wigner function $-\ln \rho = W$ at the jumping point are displayed in solid, dashed, and close-circles lines, respectively. The excitation of the displaced mode linearly depends on its displacement.

FIG. 5. Same as figure 5 with the displacement of the $C-H$ totally symmetric mode considered as a free parameter. The coordinate and the value of the Wigner function at the jumping point are plotted vs. the $C-H$ displacement between the two surfaces.

FIG. 6. Same as figures 5 and 6 with the energy gap between the electronic surfaces considered as a free parameter. The coordinate and the value of the Wigner function at the jumping point are plotted vs. the energy gap between the surfaces. The value of the Wigner function at the jumping point exponentially depends on the energy gap.

FIG. 7. Local $C-H$ stretching potentials. The harmonic, anharmonic, and Morse potentials for the local $C-H$ stretching of the S_0 and S_2 electronic states are shown in solid, dotted-dashed, and dashed lines, respectively. The anharmonicity of the upper surface is plotted here as if equal for the two electronic states, but is considered as a free parameter in the calculations.

FIG. 8. (a) Results of the calculation for the $S_2 \rightarrow S_0$ transition taking the Morse potentials for both surfaces. The coordinate and the value of the Wigner function at the jumping point are plotted vs. the anharmonicity x_e of the upper electronic surface. The excitations of the local $C-H$, totally symmetric $C-C$ stretching, normal $C-H$ stretching and the value of the Wigner function $-\ln\rho = W$ at the jumping point are displayed in solid, dotted, dashed and close-circles lines. (b) Wigner function for the Morse oscillator with $\omega = 3212\ cm^{-1}$ and different anharmonicities x_e.

FIG. 9. The two normal modes that may have non-zero displacements due to a possible pseudo-Jahn-Teller effect on the S_2 surface potential. q_6 is a ring deformation mode and q_8 is a ring stretch mode. Both modes belong to the e_{2g} representation for the D_{6h} symmetry and to the a_g representation of the D_{2h} symmetry.

FIG. 10. Results of the calculation for the $S_2 \rightarrow S_0$ transition taking the potentials of section 4.3 and including a pseudo-JT deformation of the benzene angles. The coordinate and the value of the Wigner function at the jumping point are plotted vs. the difference between the angles of the benzene molecule. The excitations of the local $C-H$, totally symmetric $C-C$ stretching, q_6 and the value of the Wigner function $-\ln\rho = W$ at the jumping point are displayed in solid, dotted, dashed and close-circles lines, respectively.

FIG. 11. Same as figure 11 but with a pseudo-JT deformation of the $C-C$ bond lengths of the benzene.

FIG. 12. The two normal modes considered here to be involved in a possible Duschinsky mode rotation. Both modes belong to the b_{2u} representation, q_{14} is a ring stretching mode, and q_{15} is a $C-H$ bending mode.

FIG. 13. Geometric demonstration of the Duschinsky mode rotation in two dimensions. The solid lines represent the contours of the Wigner initial function on the excited electronic surface. The outer dashed ellipse represents the constraint surface for the lower surface $H_F = E$. Implementation of the Duschinsky rotation is done by rotating the inner ellipse by β.

FIG. 14. Results of the calculation for the $S_2 \rightarrow S_0$ transition taking the potentials of section 4.3 and including a Duschinsky mode rotation between q_{14} and q_{15}. The coordinates and the value of the Wigner function at the jumping point are plotted vs. the rotation angle β. The excitations of the local $C-H$, totally symmetric $C-C$ stretching, q_{14}, q_{15} and the value of the Wigner function $-\ln\rho = W$ at the jumping point are displayed in solid, dashed, dotted, dotted-dashed and close-circles lines, respectively.

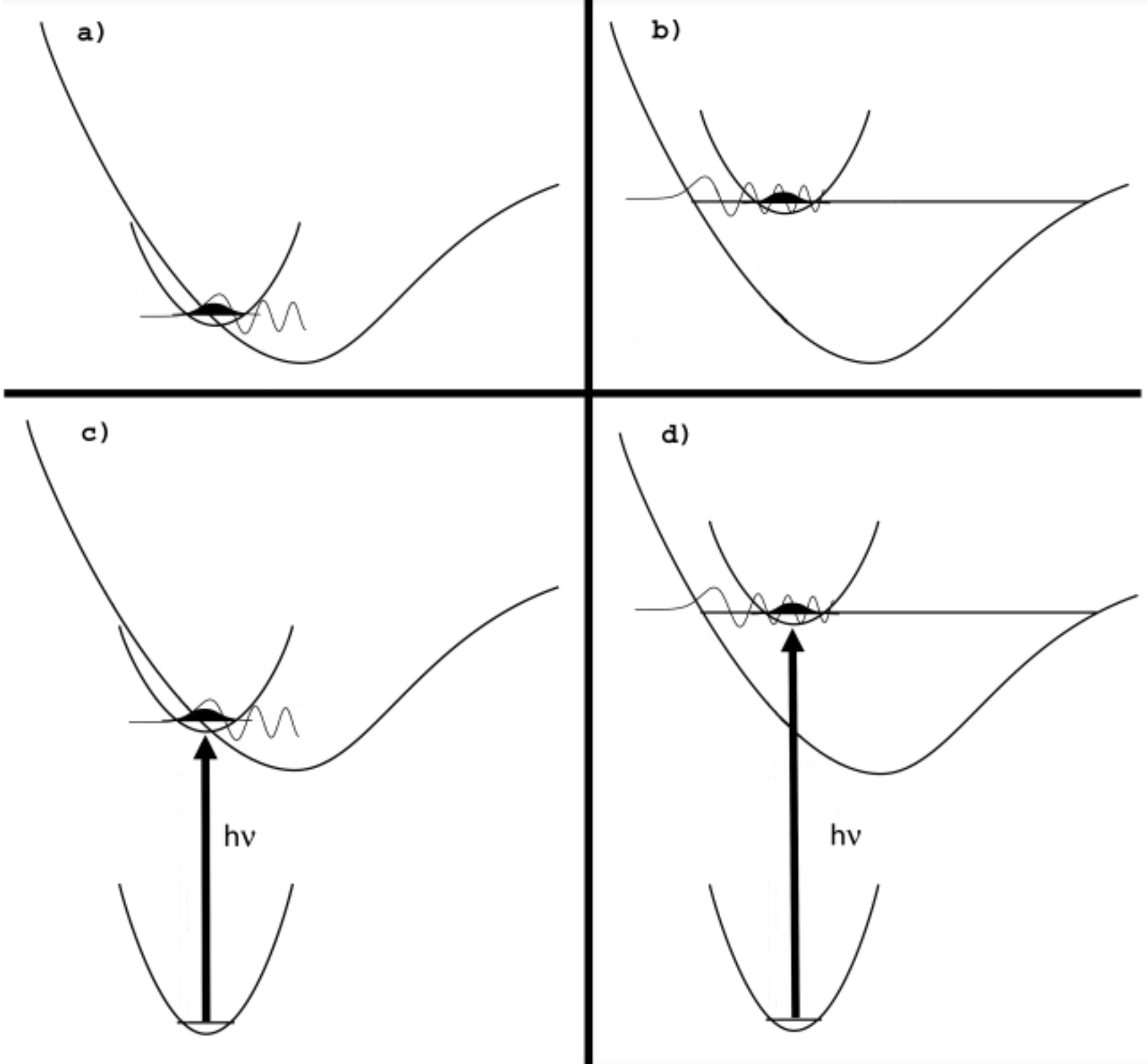
a)
b)
c)
hν
d)
hν

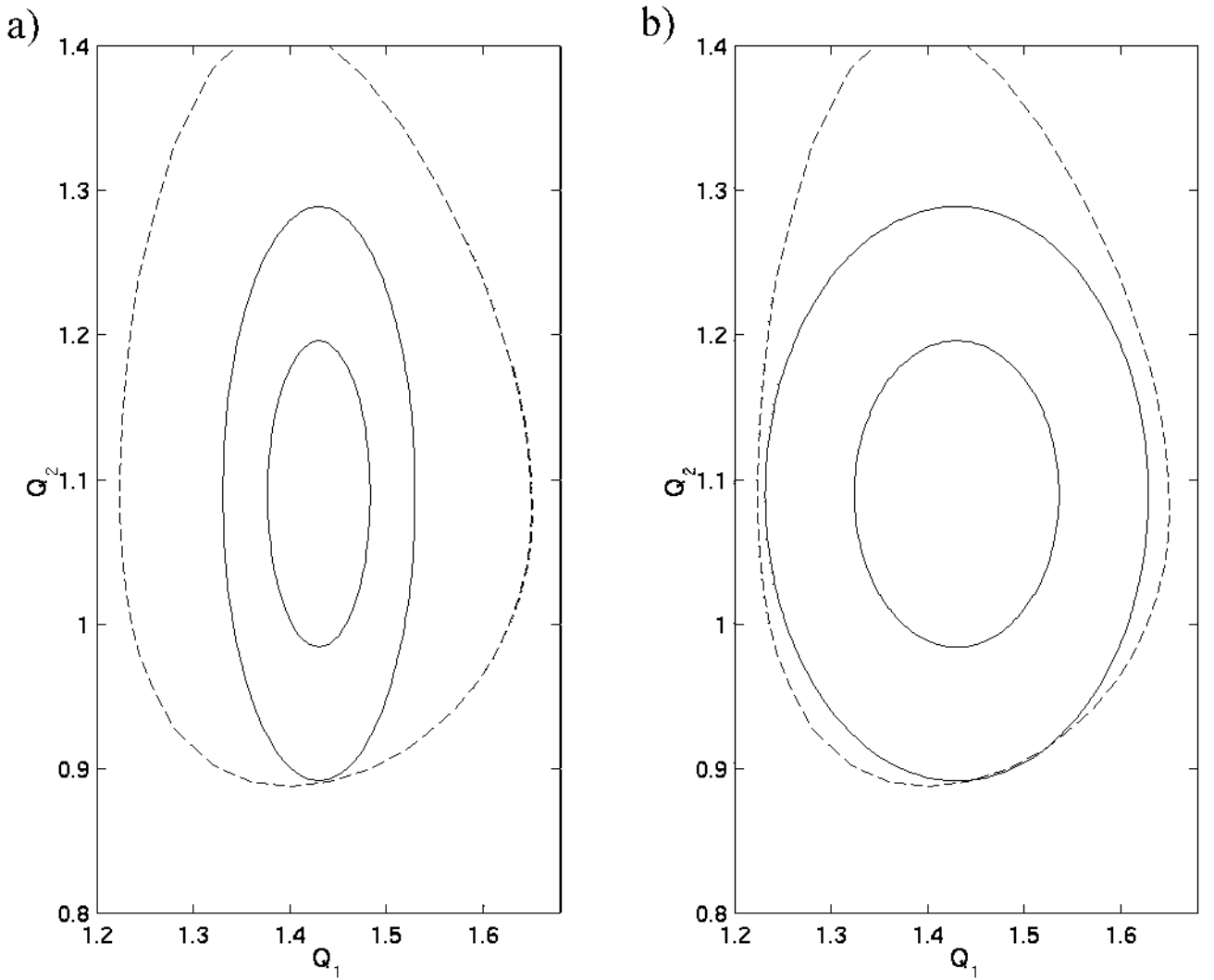
a)
b)
1.4
1.3
1.2
1.1
1
0.9
0.8
Q_2
1.2
1.3
1.4
1.5
1.6
Q_1

Non-degenerate

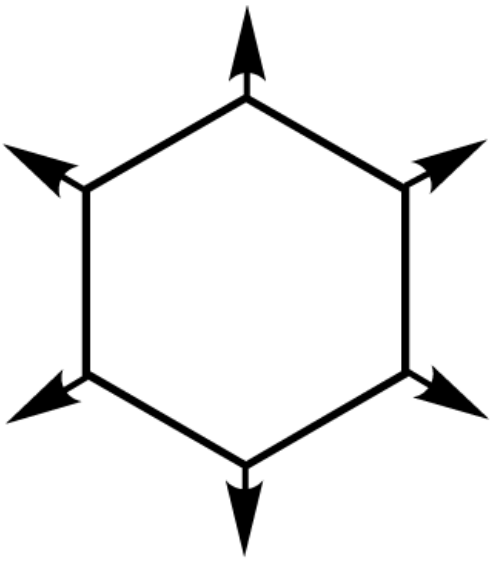

q_2

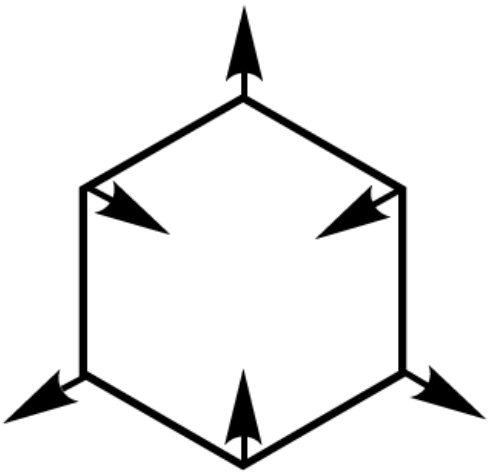

q_{13}

Degenerate

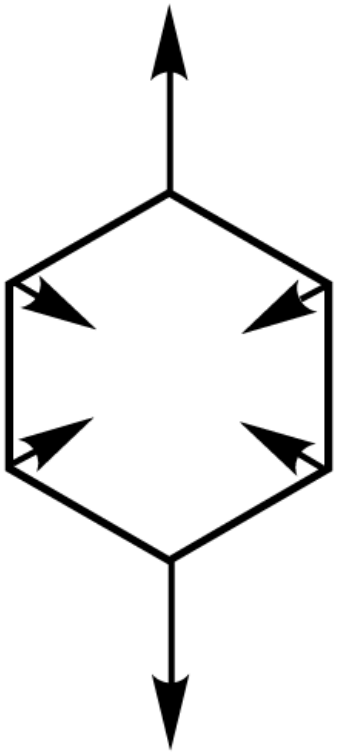

q_7

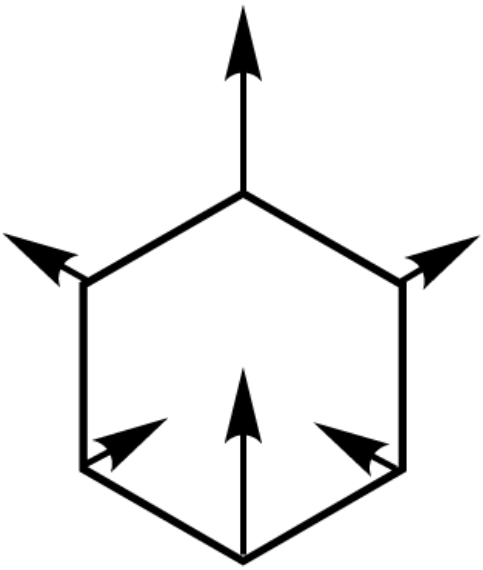

q_{20}

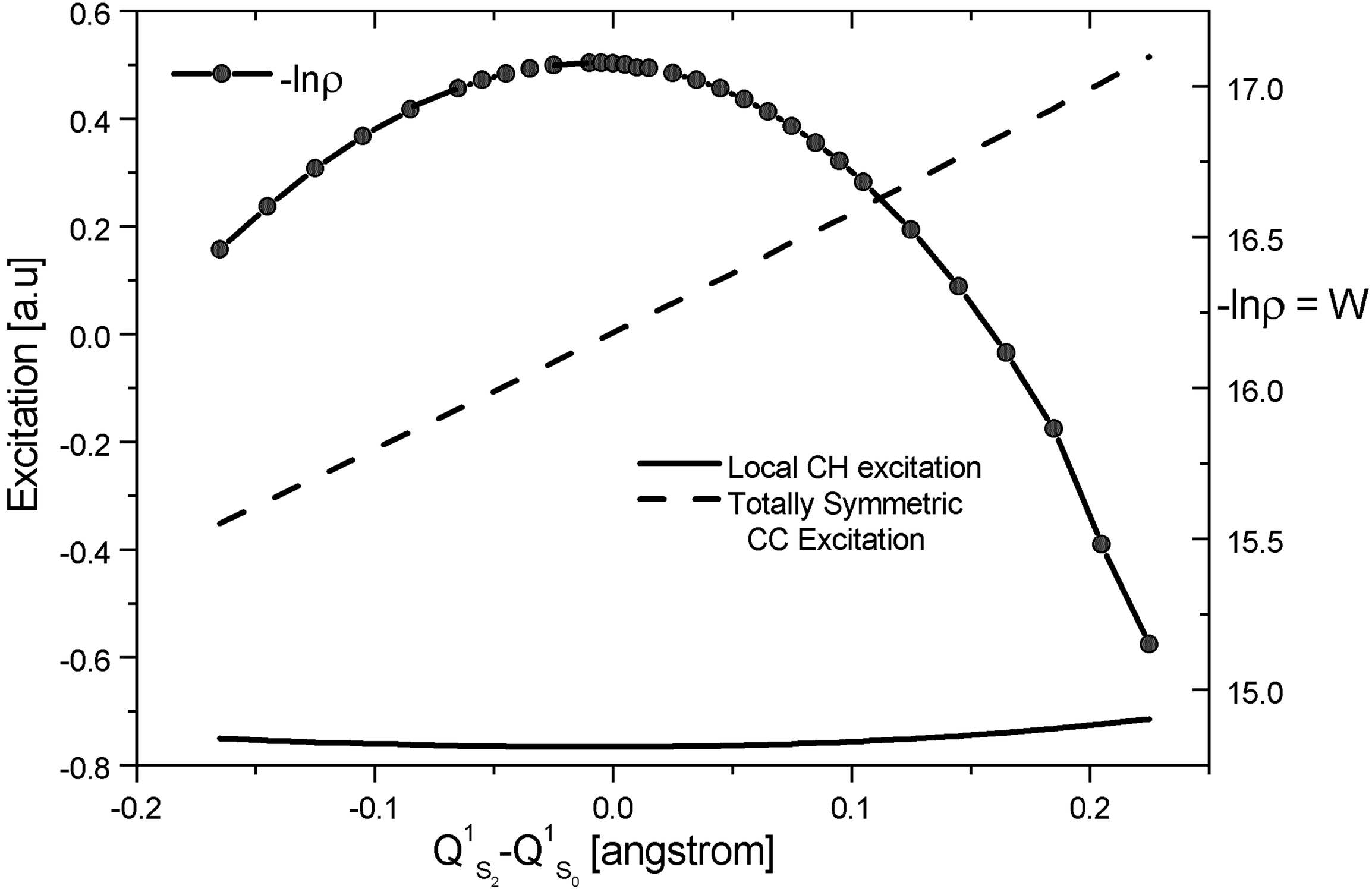
0.6
0.4
0.2
0.0
-0.2
-0.4
-0.6
-0.8
Excitation [a.u]
-lnρ
17.0
16.5
16.0
15.5
15.0
-lnρ = W
Local CH excitation
Totally Symmetric
CC Excitation
-0.2
-0.1
0.0
0.1
0.2
Q1S2-Q1S0 [angstrom]

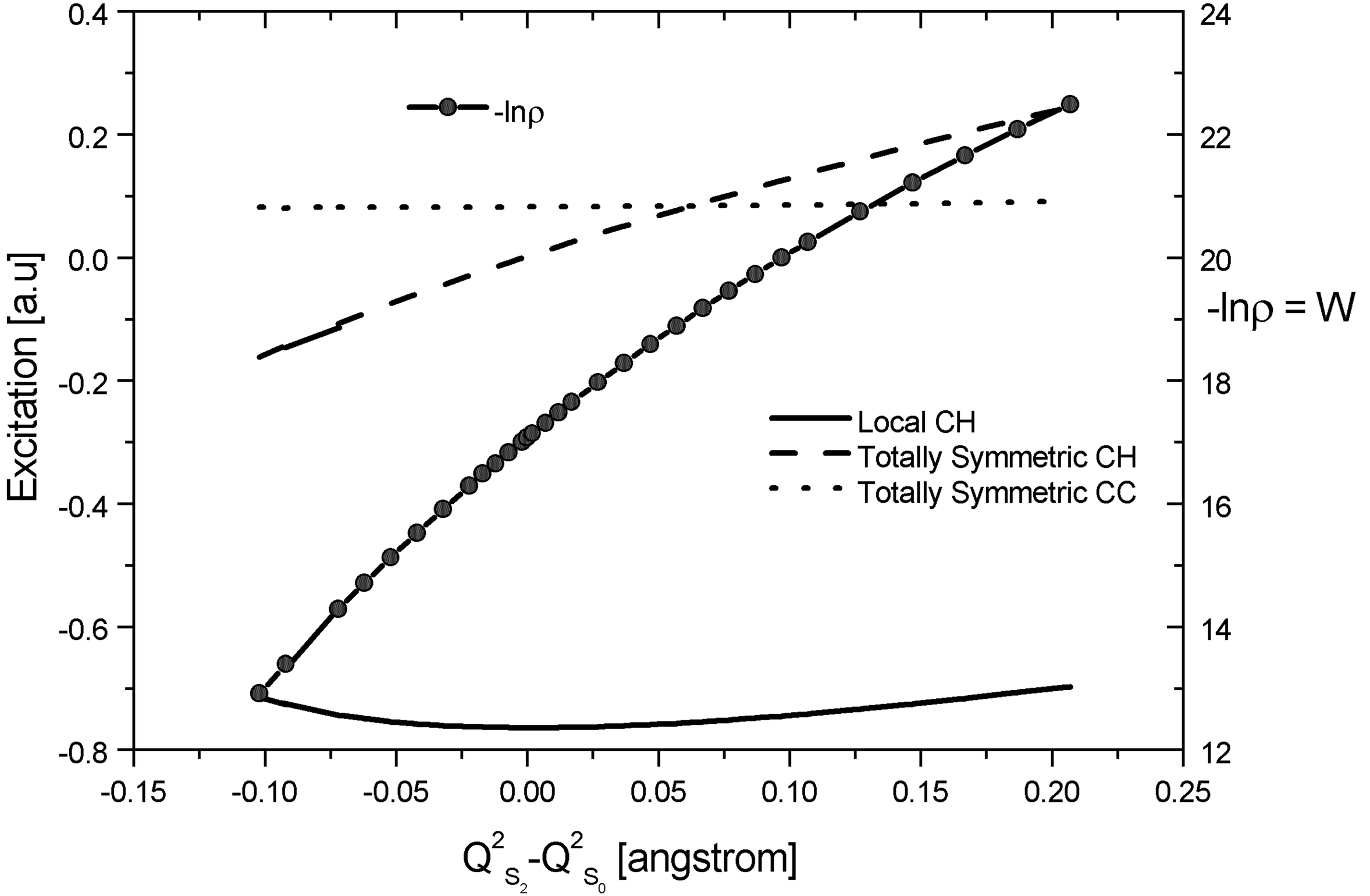
-lnρ
Local CH
Totally Symmetric CH
Totally Symmetric CC
Excitation [a.u]
-lnρ = W
$Q^2_{S_2}-Q^2_{S_0}$ [angstrom]
0.4
0.2
0.0
-0.2
-0.4
-0.6
-0.8
24
22
20
18
16
14
12
-0.15
-0.10
-0.05
0.00
0.05
0.10
0.15
0.20
0.25

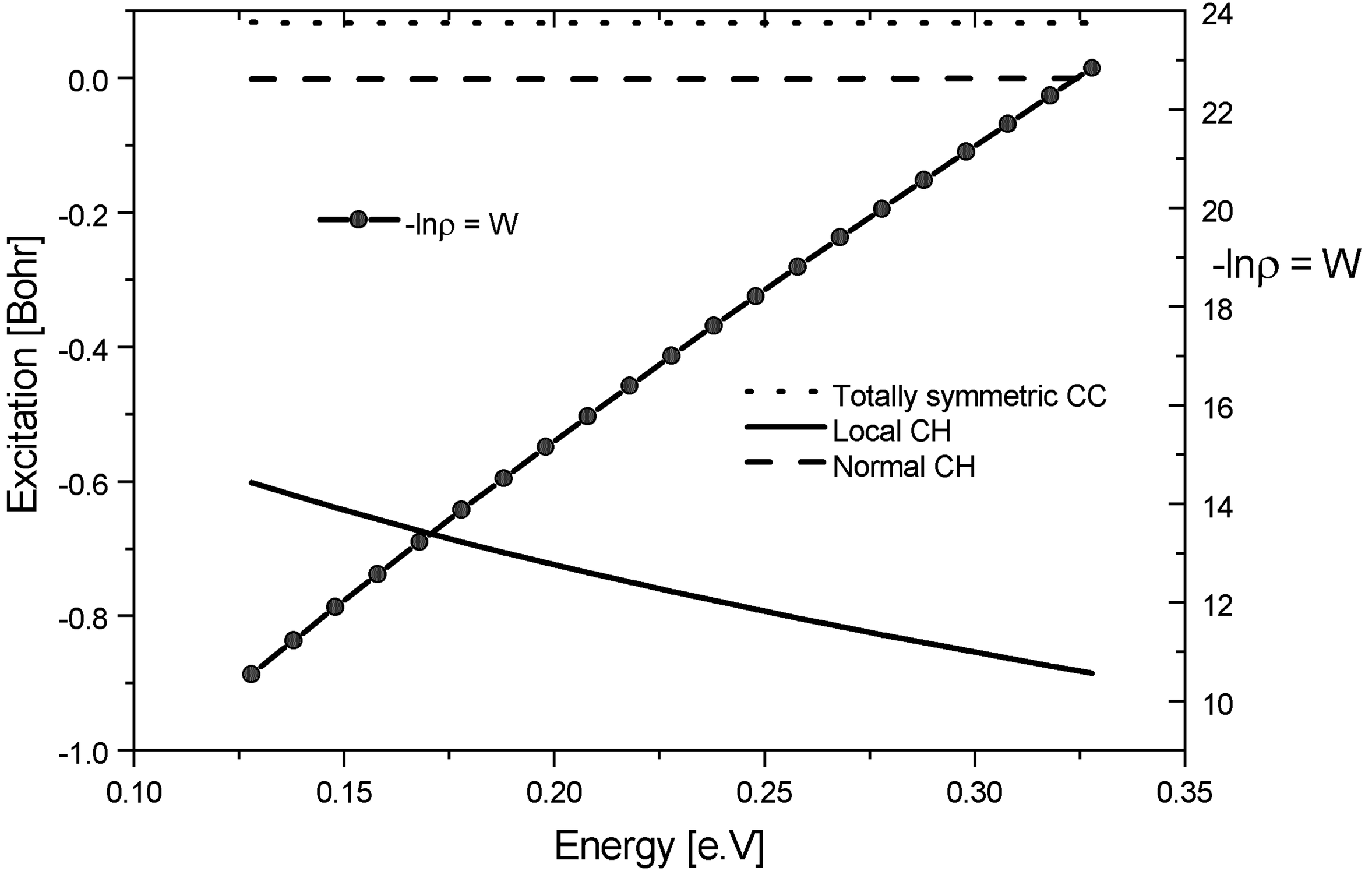
0.0
-0.2
-0.4
-0.6
-0.8
-1.0
Excitation [Bohr]
0.10
0.15
0.20
0.25
0.30
0.35
Energy [e.V]
24
22
20
18
16
14
12
10
-lnρ = W
-lnρ = W
Totally symmetric CC
Local CH
Normal CH

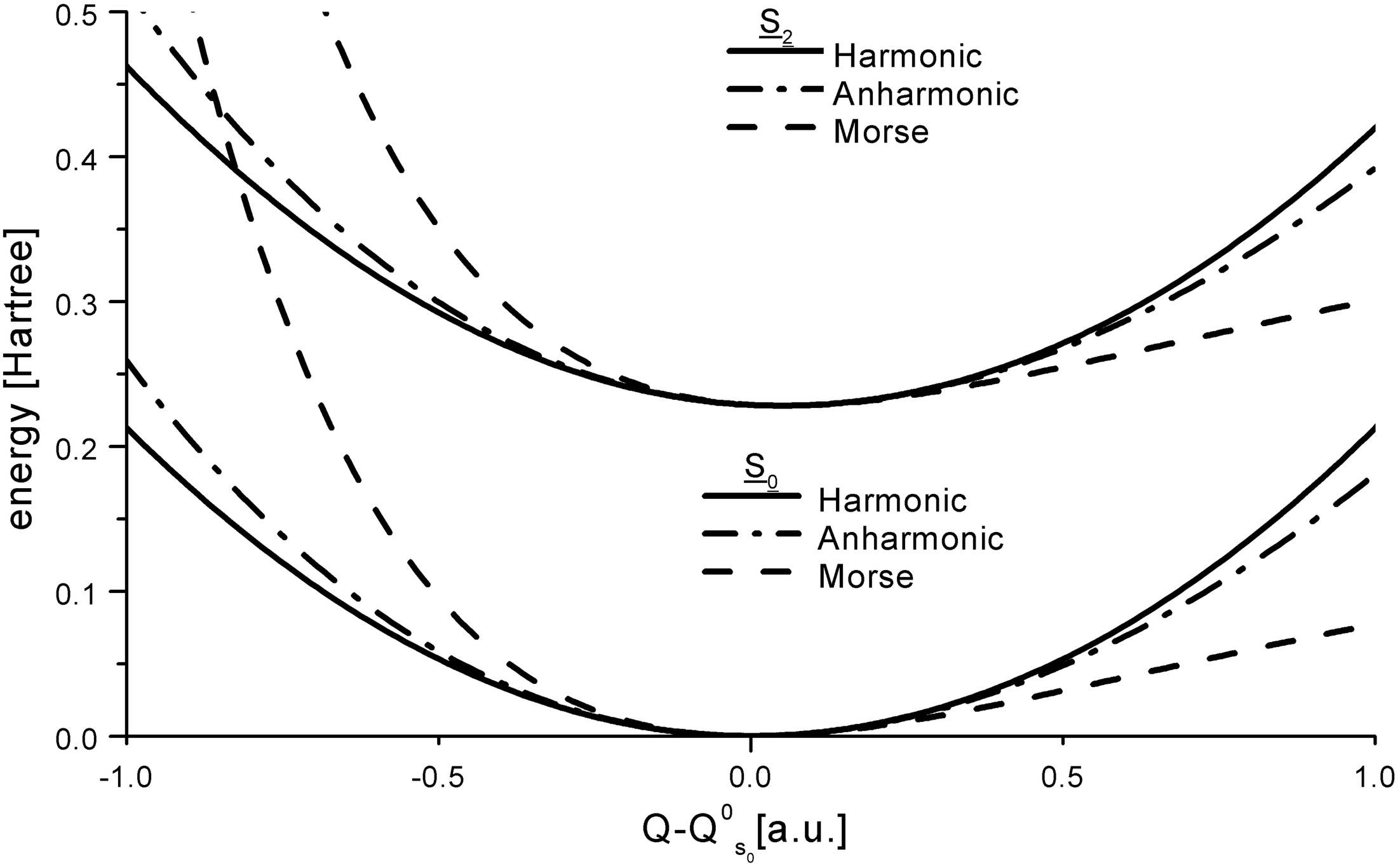
0.5
0.4
0.3
0.2
0.1
0.0
energy [Hartree]
-1.0
-0.5
0.0
0.5
1.0
Q-Q$^0_{s_0}$[a.u.]
S$_2$
Harmonic
Anharmonic
Morse
S$_0$
Harmonic
Anharmonic
Morse

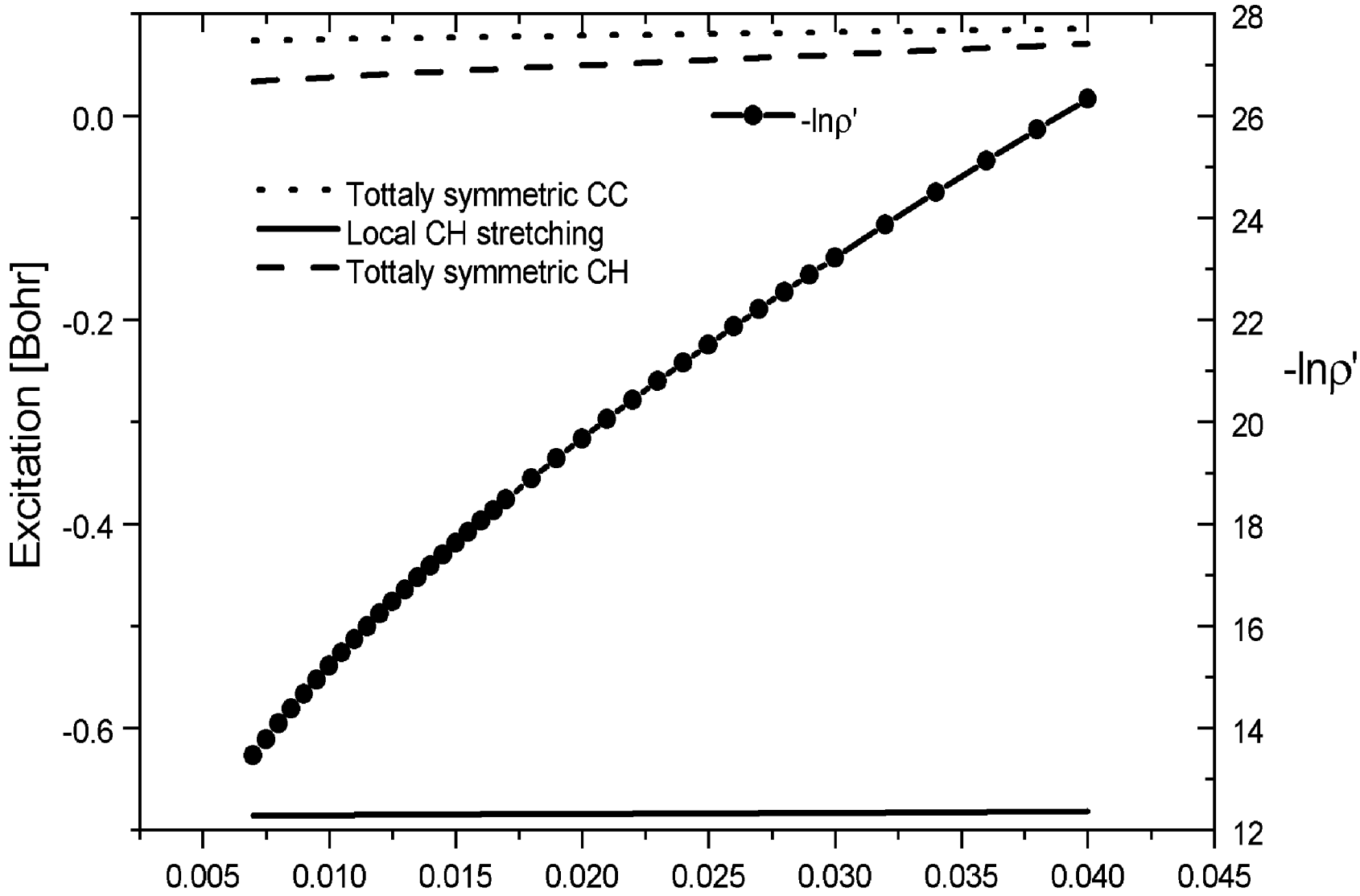
Excitation [Bohr]
0.0
-0.2
-0.4
-0.6
28
26
24
22
20
18
16
14
12
-lnρ'
-lnρ'
Tottaly symmetric CC
Local CH stretching
Tottaly symmetric CH
0.005
0.010
0.015
0.020
0.025
0.030
0.035
0.040
0.045

x_e

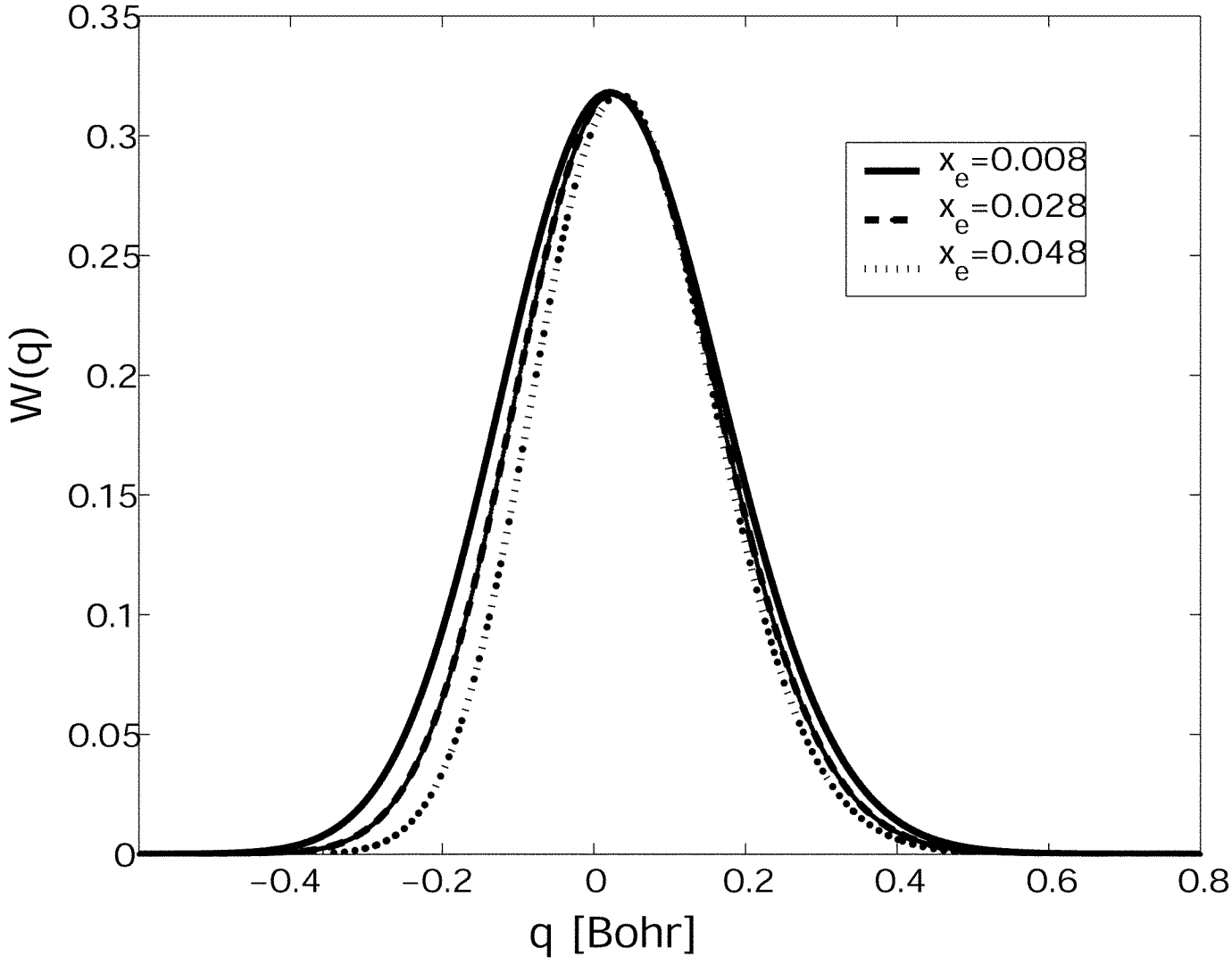
W(q)
0.35
0.3
0.25
0.2
0.15
0.1
0.05
0
x_e=0.008
x_e=0.028
x_e=0.048
−0.4
−0.2
0
0.2
0.4
0.6
0.8
q [Bohr]

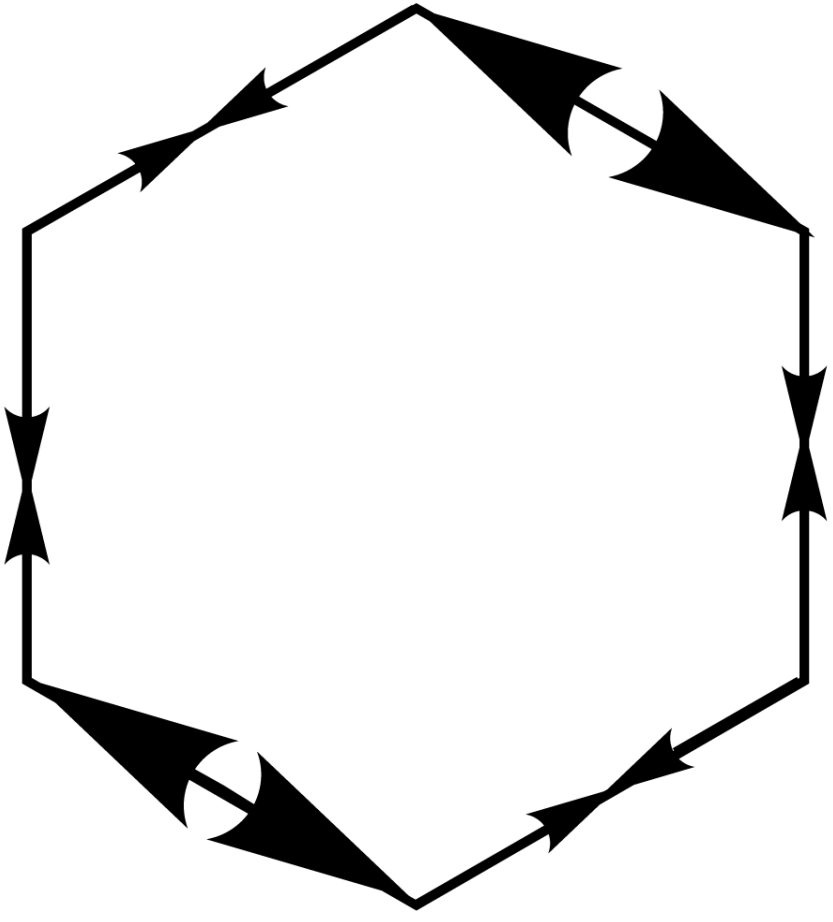

q_8

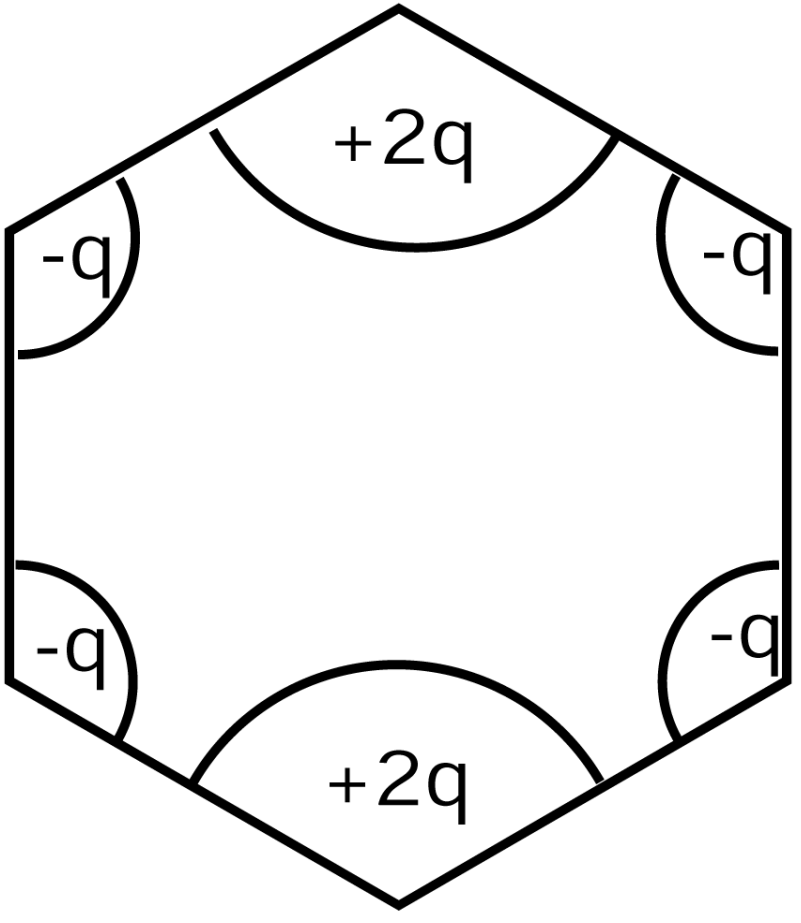

q_6

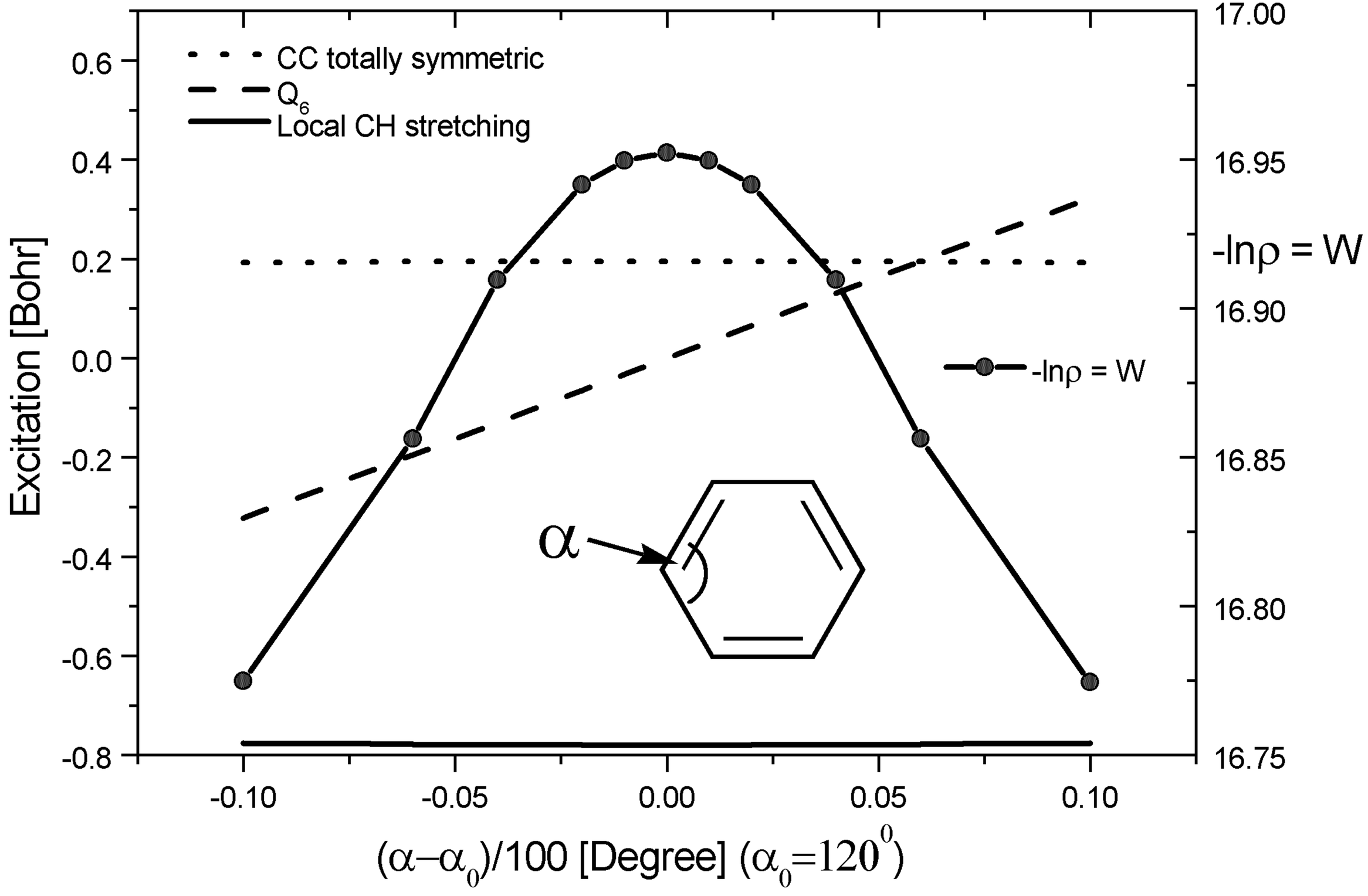
CC totally symmetric
Q_6
Local CH stretching
-lnρ = W
α
Excitation [Bohr]
0.6
0.4
0.2
0.0
-0.2
-0.4
-0.6
-0.8
17.00
16.95
16.90
16.85
16.80
16.75
-lnρ = W
-0.10
-0.05
0.00
0.05
0.10
$(\alpha-\alpha_0)/100$ [Degree] ($\alpha_0=120^0$)

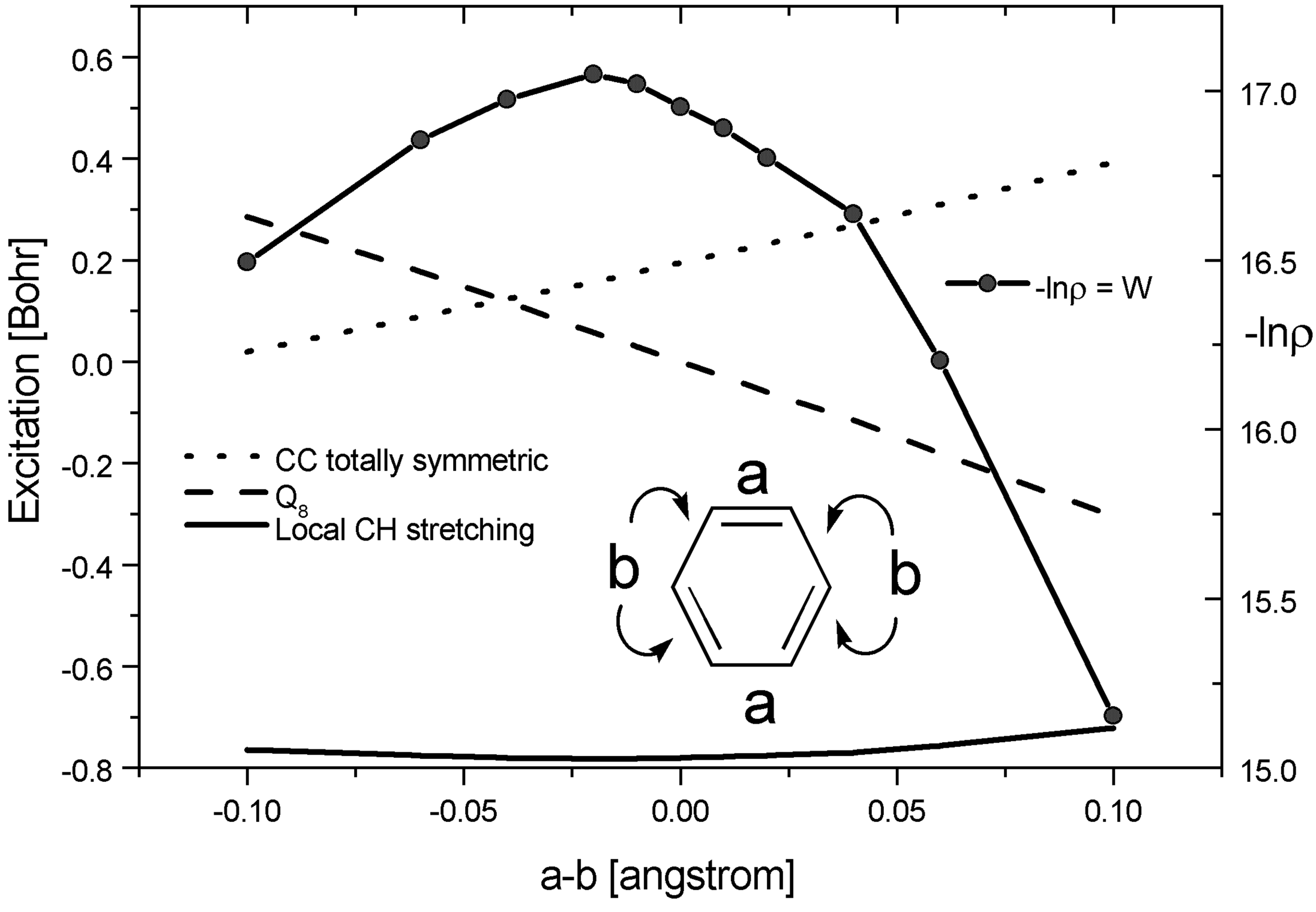
0.6
0.4
0.2
0.0
-0.2
-0.4
-0.6
-0.8
Excitation [Bohr]
17.0
16.5
16.0
15.5
15.0
-lnρ = W
-0.10
-0.05
0.00
0.05
0.10
a-b [angstrom]
CC totally symmetric
Q8
Local CH stretching
a
b
b
a

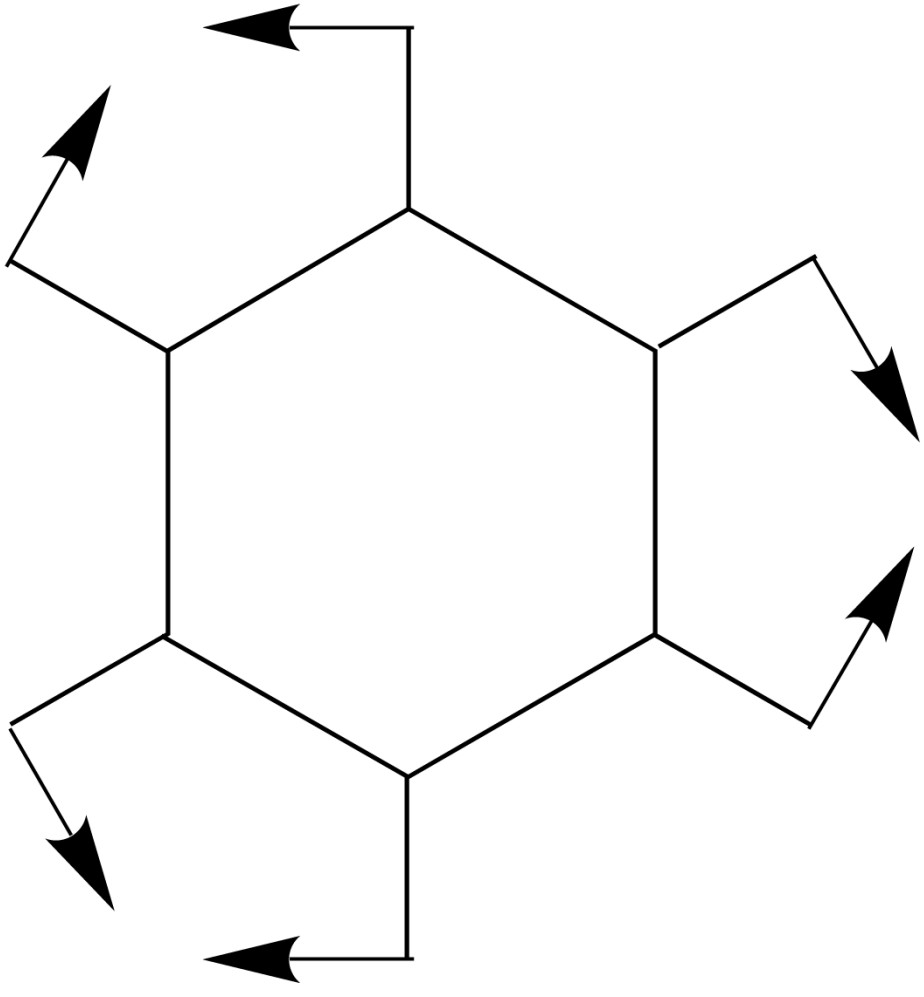

q_{14}

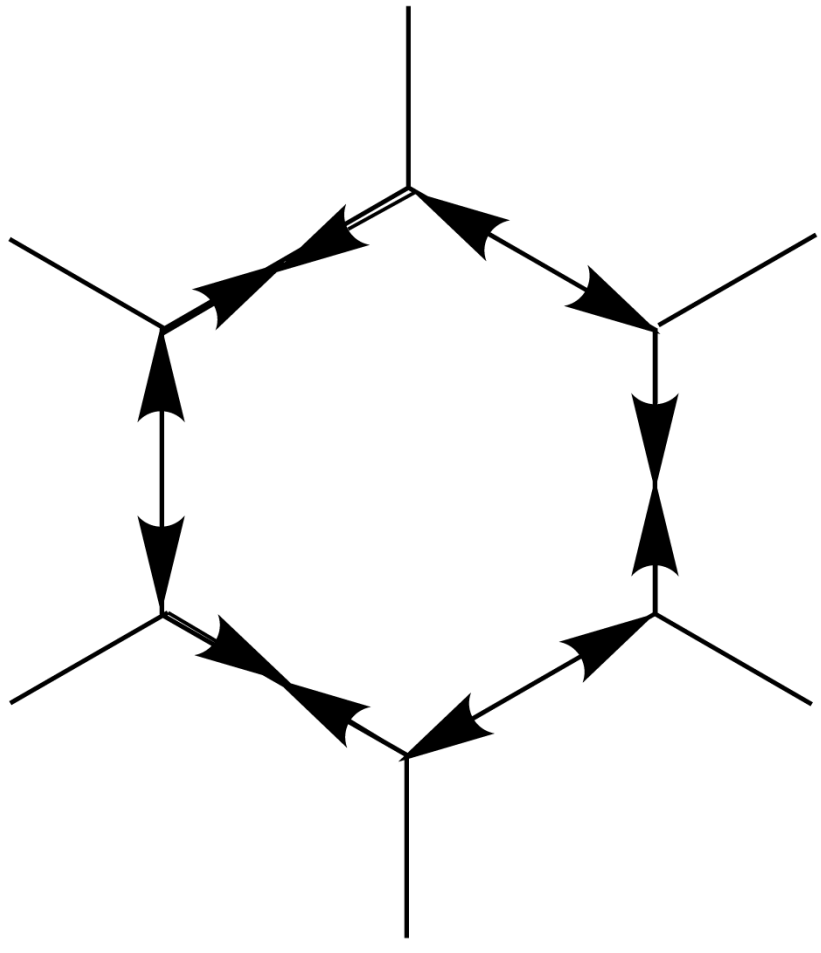

q_{15}

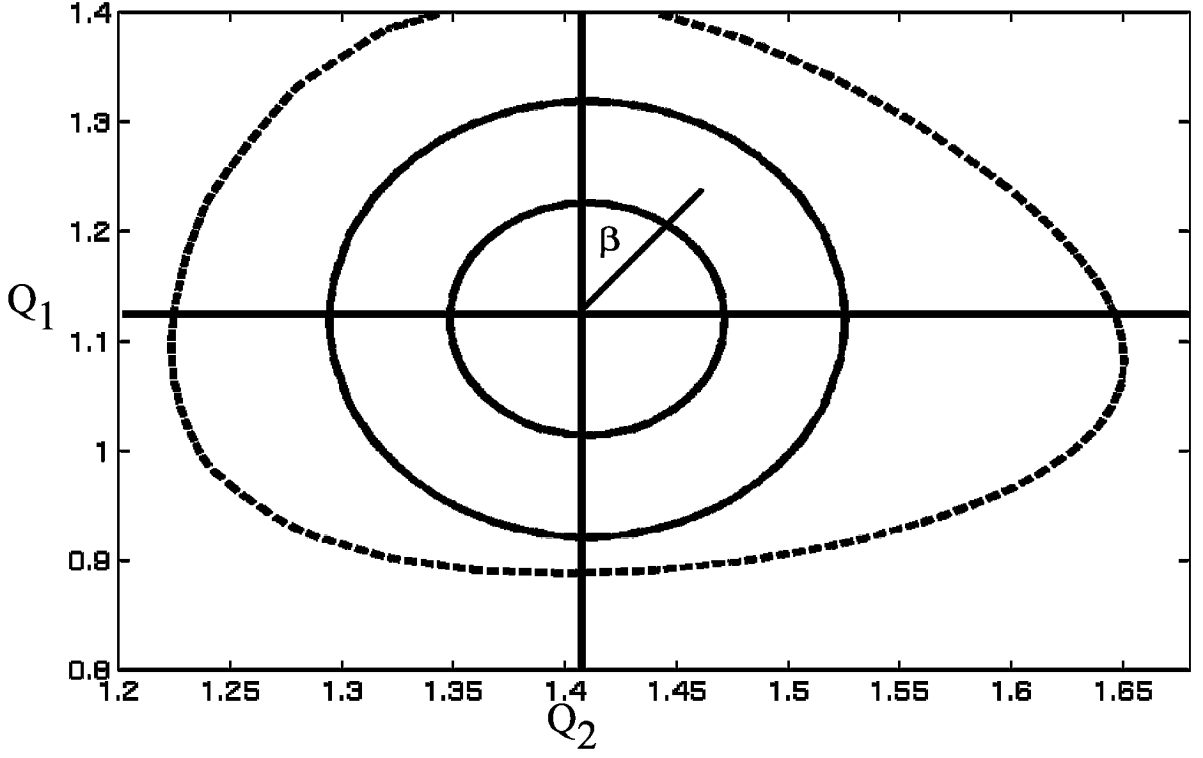
1.4
1.3
1.2
1.1
1
0.9
0.8
Q_1
β
1.2
1.25
1.3
1.35
1.4
1.45
1.5
1.55
1.6
1.65
Q_2

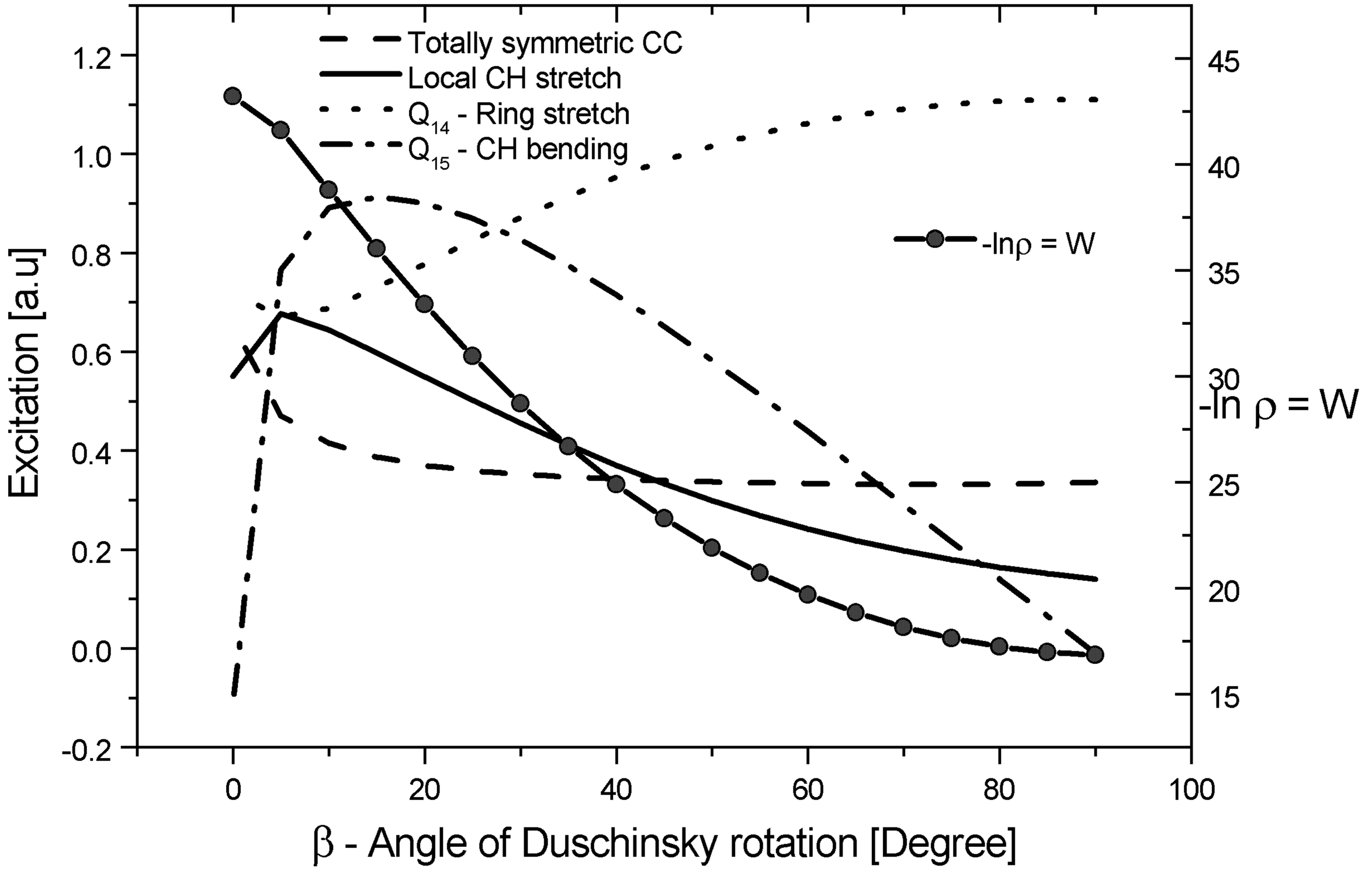
Totally symmetric CC
Local CH stretch
Q14 - Ring stretch
Q15 - CH bending
-lnρ = W
Excitation [a.u]
-ln ρ = W
β - Angle of Duschinsky rotation [Degree]
1.2
1.0
0.8
0.6
0.4
0.2
0.0
-0.2
45
40
35
30
25
20
15
0
20
40
60
80
100